HHS Public Access

Author manuscript

Cell Rep. Author manuscript; available in PMC 2020 November 12.

Published in final edited form as:

Cell Rep. 2020 October 27; 33(4): 108270. doi:10.1016/j.celrep.2020.108270.

Endocannabinoid Receptor-1 and Sympathetic Nervous System Mediate the Beneficial Metabolic Effects of Gastric Bypass

Yuanchao Ye[1,21], **Marwa Abu El Haija**[2,21], **Donald A. Morgan**[3], **Deng Guo**[3], **Yang Song**[4], **Aaron Frank**[5], **Liping Tian**[6], **Ruth A. Riedl**[3], **Colin M.L. Burnett**[1,3], **Zhan Gao**[1], **Zhiyong Zhu**[1], **Shailesh K. Shahi**[7], **Kasra Zarei**[8], **Anne Couvelard**[9,10], **Nicolas Poté**[9,10], **Lara Ribeiro-Parenti**[9,11], **André Bado**[9], **Lama Noureddine**[1], **Andrew Bellizzi**[7], **Paul Kievit**[12], **Ashutosh K. Mangalam**[7,13], **Leonid V. Zingman**[1,14,15,16], **Maude Le Gall**[9], **Justin L. Grobe**[17], **Lee M. Kaplan**[18,19], **Deborah Clegg**[20], **Kamal Rahmouni**[1,3,8,14,15,16], **Mohamad Mokadem**[1,3,14,15,16,22,*]

[1]Department of Internal Medicine, University of Iowa Carver College of Medicine, Iowa City, IA 52242, USA

[2]Department of Pediatrics, Division of Gastroenterology, Hepatology, and Nutrition, Stanford University School of Medicine, Palo Alto, CA 94304, USA

[3]Department of Neuroscience and Pharmacology, University of Iowa Carver College of Medicine, Iowa City, IA 52242, USA

[4]College of Pharmacy, China Medical University, 77 Puhe Rd., Liaoning 110122, P.R. China

[5]The Biomedical Research Department, Diabetes and Obesity Research Division, Cedars Sinai Medical Center, Beverly Hills, CA 90048, USA

[6]Department of Clinical Pharmacy, School of Basic Medicine and Clinical Pharmacy, China Pharmaceutical University, Nanjing, Jiangsu 211198, P.R. China

[7]Department of Pathology, University of Iowa Carver College of Medicine, Iowa City, IA 52242, USA

[8]Medical Scientist Training Program, University of Iowa Carver College of Medicine, Iowa City, IA 52242, USA

[9]INSERM U1149, Centre de Recherche sur l'Inflammation, Université de Paris, Paris 75018, France

*Correspondence: mohamad-mokadem@uiowa.edu.

AUTHOR CONTRIBUTIONS

Conceptualization, Y.Y., M.A.E.H., and M.M.; Formal Analysis, Y.Y., M.A., D.A.M., A.F., S.K.S., K.Z., A.C., N.P., A. Bado, A. Bellizzi, Z.G., Z.Z.; Investigation, Y.Y., M.A.E.H., D.A.M., Y.S., A.F., L.T., R.A.R., Z.G., Z.Z., S.K.S., K.Z., A.C., N.P., L.R.-P., A. Bado, A. Bellizzi, P.K., A.K.M., L.V.Z., M.L.G., J.L.G., D.C., K.R., and M.M.; Resources, C.M.L.B., L.N.; Writing, Y.Y., M.A.E.H., and M.M.; Critical Revision, Y.Y., K.R., and M.M.; Supervision, P.K., A.K.M., L.V.Z., M.L.G., J.L.G., L.M.K., D.C., K.R., and M.M.; Funding Acquisition, A.K.M., L.V.Z., M.L.G., J.L.G., L.M.K., D.C., K.R., and M.M.

DECLARATION OF INTERESTS

The authors declare no competing interests.

SUPPLEMENTAL INFORMATION

Supplemental Information can be found online at https://doi.org/10.1016/j.celrep.2020.108270.

[10]Department of Pathology, Bichat Hospital, AP-HP, Paris 75018, France

[11]Department of General and Digestive Surgery, Bichat Hospital, AP-HP, Paris 75018, France

[12]Division of Diabetes, Obesity and Metabolism, Oregon National Primate Research Center, Oregon Health and Science University, Beaverton, OR 97006, USA

[13]Interdisciplinary Graduate Program in Immunology and Molecular Medicine, University of Iowa Carver College of Medicine, Iowa City, IA 52242, USA

[14]Fraternal Orders of Eagles Diabetes Research Center, Iowa City, IA 52242, USA

[15]Veterans Affairs Health Care System, Iowa City, IA 52242, USA

[16]Obesity Research & Education Initiative, University of Iowa, Iowa City, IA 52242, USA

[17]Departments of Physiology and Biomedical Engineering, Medical College of Wisconsin, Milwaukee, MI 53226, USA

[18]Department of Medicine, Harvard Medical School, Boston, MA 02115, USA

[19]Obesity, Metabolism, and Nutrition Institute, Massachusetts General Hospital, Boston, MA 02114, USA

[20]College of Nursing and Health Professions, Drexel University, 1601 Cherry Street, Philadelphia, PA 19102, USA

[21]These authors contributed equally

[22]Lead Contact

SUMMARY

The exact mechanisms underlying the metabolic effects of bariatric surgery remain unclear. Here, we demonstrate, using a combination of direct and indirect calorimetry, an increase in total resting metabolic rate (RMR) and specifically anaerobic RMR after Roux-en-Y gastric bypass (RYGB), but not sleeve gastrectomy (SG). We also show an RYGB-specific increase in splanchnic sympathetic nerve activity and “browning” of visceral mesenteric fat. Consequently, selective splanchnic denervation abolishes all beneficial metabolic outcomes of gastric bypass that involve changes in the endocannabinoid signaling within the small intestine. Furthermore, we demonstrate that administration of rimonabant, an endocannabinoid receptor-1 (CB1) inverse agonist, to obese mice mimics RYGB-specific effects on energy balance and splanchnic nerve activity. On the other hand, arachidonoylethanolamide (AEA), a CB1 agonist, attenuates the weight loss and metabolic signature of this procedure. These findings identify CB1 as a key player in energy regulation post-RYGB via a pathway involving the sympathetic nervous system.

In Brief

Ye et al. show that energy regulation differs between Roux-en-Y gastric bypass (RYGB) and sleeve gastrectomy (SG) where only RYGB enhances splanchnic nerve activity, to induce visceral fat thermogenesis, and increases resting metabolic rate (RMR). This sympathetic-mediated “browning” of visceral fat seems to be dependent on endocannabinoid receptor-1 (CB1) signaling.

Graphical Abstract

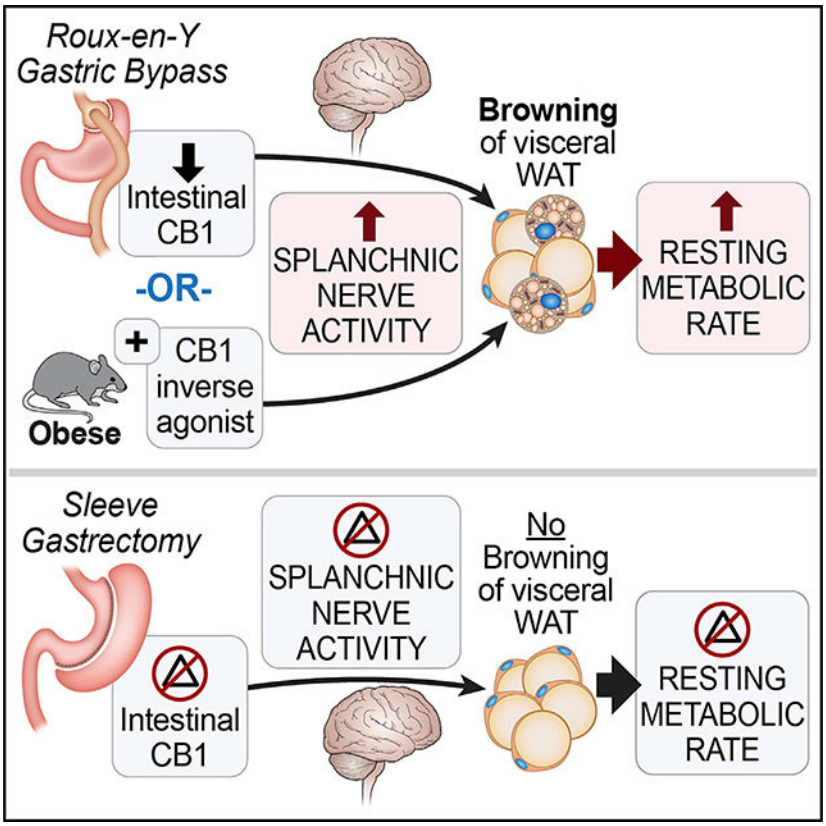

INTRODUCTION

The growing epidemic of obesity is projected to surpass starvation as the main global health concern by 2030 (González-Muniesa et al., 2017). Furthermore, the percentage of people with morbid obesity (i.e., body mass index [BMI] > 40) has increased by more than 300% in the past decade (Sturm and Hattori, 2013). While few effective therapies exist for the management of morbid obesity and its associated metabolic disorders such as type 2 diabetes, bariatric surgery has demonstrated its superiority over pharmacological and behavioral therapies (Adams et al., 2017; Schauer et al., 2017). Roux-en-Y gastric bypass (RYGB) is one of the most effective and commonly performed bariatric procedures that can carry long-lasting metabolic benefits (Adams et al., 2017; Puzziferri et al., 2014; Schauer et al., 2017). It should be noted that data regarding weight loss and long-term weight maintenance after sleeve gastrectomy (SG)—the other most common bariatric procedure—is rather poor compared with RYGB (Adams et al., 2017; Buchwald et al., 2004; Maciejewski et al., 2016; Puzziferri et al., 2014; Sjöström et al., 2007). The anatomical rearrangement of the small intestine is the main difference between RYGB and SG, suggesting a vital role of the small intestine in regulation of energy homeostasis and likely in long-term weight maintenance. Understanding the mechanisms underlying weight and metabolic regulation post-RYGB can facilitate future development of less invasive therapies for obesity in individuals who do not meet the criteria for surgery. On the other hand, it has been suggested

that both RYGB and SG might have more metabolic and mechanistic similarities than would be expected from their anatomical rearrangement. This is due to the fact that they can reproduce similar physiologic, behavioral, and hormonal responses that other bariatric surgeries such as adjustable gastric banding and vertical band gastroplasty cannot evoke (Seeley et al., 2015; Stefater et al., 2012). Many studies in rodents suggested that RYGB can induce an increase in total energy expenditure, measured at different time points using indirect calorimetry or a validated mathematical formula, compared with *ad-libitum*-fed shams and weight-matched shams (Hao et al., 2017; Zechner et al., 2013). One study suggested that despite the decrease in food intake after SG, there was no difference in total energy expenditure—measured by indirect calorimetry—between SG-operated rats and their sham counterparts (Stefater et al., 2010). Yet, another study showed that pair feeding (PF) alone is sufficient to weight-matched sham-operated animals with their SG counterparts (Hao et al., 2017). It was previously suggested that when using indirect calorimetry for calculation of thermal equivalents (in multiple species) the absolute error can reach as high as 38% compared with the gold standard direct calorimetry (Walsberg and Hoffman, 2005). Since most previous bariatric studies used indirect calorimetry or a calculated formula—founded on it—many still debate the true contribution of total energy expenditure to weight loss after bariatric surgery, specifically RYGB and SG. To elucidate the mechanisms by which each of these bariatric surgical procedures regulates energy balance, we used a comprehensive approach that includes a combination of sensitive direct and indirect calorimetry in two mouse models of RYGB and SG to accurately measure total energy expenditure and resting metabolic rate (RMR).

RESULTS

RYGB, but Not SG, Increases RMR and vWAT Thermogenesis

RYGB-caused substantial body weight loss is observed in diet-induced obese (DIO) mice (Figure S1A). This reduction in body mass cannot be explained by the transient decrease in food intake (Figures S1B and S1C). Furthermore, RYGB induces a significant reduction in feeding efficiency, defined as weight gained per energy consumed (Figure S1D). However, the slight increase in fecal caloric loss (~1 kcal/day) observed in RYGB-operated mice (Figure S1E) did not correlate with the amount of total body weight loss (Figure S1F). On the other hand, total energy expenditure (assessed by 24-h indirect calorimetry using the Comprehensive Lab Animal Monitoring System [CLAMS]) increases at post-week 3 after RYGB (Figure S1G) despite a decrease in serum leptin concentration (Figure S1H). This suggests that weight loss post-RYGB is likely due to a primary central process that resets a new energy balance target, as previously suggested (Mokadem et al., 2013, 2015). On the other hand, SG induces a smaller but significant decrease in body weight accompanied by a reduction in average daily food intake (Figures S2A and S2B). However, no significant changes in feeding efficiency or total energy expenditure were noted after SG (Figures S2C and S2D) despite the decrease in serum leptin levels and improvement in glucose homeostasis as in RYGB (Figures S2E–S2G) (Hao et al., 2017).

Next, we used a highly sensitive direct calorimetry method to determine the contribution of RMR to the increased total energy expenditure evoked by RYGB (Burnett and Grobe, 2013,

2014; Pittet et al., 1974, 1976; Walsberg and Hoffman, 2005). We also took advantage of the sensitivity of direct calorimetry to analyze the effect of SG on energy expenditure that could have been missed by respirometry. Respirometry (or indirect calorimetry) estimates energy expenditure or "heat production" by assuming that all energy processes within the body are "aerobic" (i.e., requiring O_2 and producing CO_2). Therefore, respirometry is practically blind to non-aerobic processes, whereas direct calorimetry represents a measure of "total" energy metabolism because this method is not biased toward any type of fuel. By default, the difference in energy measurement between direct calorimetry (representing "total RMR") and indirect calorimetry (representing "aerobic RMR") would be labeled as "anaerobic RMR." We studied two groups of DIO mice (RYGB and SG) after post-operative week 2 when their body weights were grossly similar (Figure 1A). Remarkably, total RMR, as measured by direct calorimetry, was significantly increased after RYGB, but not after SG (Figure 1B). Anaerobic RMR, calculated from direct and indirect calorimetry measurements, was also increased only after RYGB surgery, accounting for ~7% of the total RMR (Figure 1C).

To explore the tissue(s) responsible for the RYGB-induced energy dissipation, we screened multiple organs involved in thermogenesis. Given the previous findings in female mice (Neinast et al., 2015), we considered the possibility that RYGB may activate brown adipose tissue (BAT) or promote the "beiging/browning" of subcutaneous white adipose tissue (scWAT), and/or visceral mesenteric white adipose tissue (vWAT). However, we found no significant change in gene expression of uncoupling protein 1 (*Ucp1*) or *Prdm16* within scWAT (Figures 1D and 1E). Furthermore, we noted a decrease in *Ucp1* expression within BAT (Figure 1D). To further assess BAT activity post-RYGB, we measured the surface body temperature around the inter-scapular area using a high-resolution infrared camera. Consistent with *Ucp1* expression, we found a decrease in surface heat generation around the inter-scapular area in RYGB-operated mice compared with sham counterparts (Figure 1F). On the other hand, Ucp1 expression was considerably elevated within vWAT, at the mRNA and protein levels, in male DIO mice after RYGB (Figures 1D and 1G). Consistent with the above-mentioned findings, *Prdm16* gene expression was significantly elevated in vWAT after RYGB (Figure 1E). These results suggest that increase of browning within vWAT rather than BAT activity is the main source of energy expenditure after RYGB. We then performed a radiolabeled glucose uptake analysis using ^{18}Fluoro-deoxyglucose (FDG) combined with positron emission tomography (PET) scanning. Interestingly, relative to the weight-matched sham controls, RYGB-operated mice displayed a significantly higher FDG uptake in the gut, specifically around the area of the small intestine (mean standardized uptake value [SUV] change in RYGB 3.239 ± 0.332 versus weight-matched shams 2.304 ± 0.233; $p < 0.05$) (Figure 1H). Taken together, these findings suggest that RYGB, but not SG, evokes its beneficial effects on energy balance by inducing thermogenesis, leading to an increase in RMR in DIO male mice. Furthermore, browning of vWAT is the main source of energy dissipation and increase in RMR post-RYGB.

RYGB, but Not SG, Evokes an Increase in the Gut's Sympathetic Nerve Activity to Induce "Browning" of vWAT

The importance of the sympathetic nervous system in the control of energy expenditure and *Ucp1* gene expression led us to assess markers of sympathetic tone within the gut. We found a significant increase in tyrosine hydroxylase (TH) expression within the Roux limb (or jejunum) and vWAT of RYGB-operated obese mice (Figures 2A and 2B), but not in SG-operated mice (Figures S3A and S3B). A similar increase in TH expression was found in non-human primates (DIO rhesus macaque monkeys) post-RYGB (Figure 2C). An increase in TH and ADBR3 protein expression was also detected in the small intestine of humans with obesity, 1–5 years after RYGB, compared with controls at the time of the surgery (Figure 2D; Table S1). On the other hand, TH expression and distribution within the layers of the stomach (as part of the alimentary tract in SG) were similar in obese human subjects before and after SG operation (Figure S3C).

The increase in TH expression within the small intestine of obese mice post-RYGB was not accompanied by change in expression of calcitonin gene-related peptide (CGRP) expression (Figures 2B and S4A), suggesting that this is not a nociception-mediated response. Additionally, levels of *Adrb3* mRNA were elevated in the alimentary tract (as opposed to the excluded bilio-pancreatic tract) of RYGB-operated mice, but not in BAT or scWAT (Figure S4B). Furthermore, TH protein expression was significantly increased in vWAT (Figure 2B), but not in scWAT, post-RYGB, pointing to activation of the sympathetic nerves subserving the gut of RYGB-operated mice (Figure S4C). On the other hand, analysis of expression of *Ucp1* and *Adrb3* genes within multiple tissues of SG-operated mice did not show any evidence of sympathetically mediated thermogenesis (Figure S3D). Together, these findings suggest that the increase in RMR and the gut's sympathetic nerve activity are specific to the RYGB surgery (i.e., its intestinal anatomical rearrangement) and not necessarily due to weight loss itself.

To further explore our hypothesis, we directly measured the sympathetic nerve activity from the greater splanchnic nerve, one of the major pre-ganglionic branches of the splanchnic bed that provides sympathetic innervation to the proximal gut and midgut (Nakano et al., 2009). Consistent with the increased intestinal expression of TH and *Adrb3*, basal splanchnic sympathetic nerve activity was significantly elevated in RYGB-operated mice compared with sham controls 1 week after surgery when the mice had similar body weights (Figure 3A) as well as 6 weeks after surgery when their body weights had segregated (Figure 3B). The splanchnic nerve carries paired fibers: (1) afferent sensory neurons from the gut to the central nervous system and (2) sympathetic autonomic efferent motor neurons projecting from the intermediolateral nucleus (IML) and synapsing in the celiac ganglion before proceeding to the targeted organ (Baron et al., 1985; Berthoud et al., 2004). In order to gauge whether the RYGB-induced increase in splanchnic nerve activity is due to an increase in afferent or efferent fiber activity, we cut distal to the recording site to specifically measure the efferent sympathetic nerve activity (Figure 3C). RYGB-operated mice displayed higher efferent sympathetic nerve activity than their sham counterparts (Figure 3D). These findings are consistent with the elevation in TH expression within jejuna of RYGB-operated animals without change in CGRP expression (Figures 2A and 2B and S4A). Interestingly, we

observed no change in the sympathetic nerve activity or TH protein expression within BAT after RYGB surgery (Figures 3E and 3F). These findings indicate that the increased sympathetic tone post-RYGB is selective to the luminal gut. This is further supported by the fact that RYGB-induced increase in TH expression within jejuna and vWAT (Figures 2A and 2B) was associated with decreased TH expression in the pancreas (Figure S4D).

Selective SpDNV Abolishes RYGB-Induced Changes in Energy Expenditure, Glucose Homeostasis, and vWAT Thermogenesis

To examine the contribution of the sympathetic nerve activity subserving the gut to the beneficial effects of RYGB on energy balance, we performed selective splanchnic denervation (SpDNV) of the luminal gut by carefully severing both the lesser splanchnic nerves, bilaterally, followed by removal of the celiac ganglia (Figures S5A and S5B). This careful maneuver did not disrupt the sympathetic innervation of the kidney, adrenal glands, or their function (Figures S5C–S5F). We subjected a group of RYGB- and sham-operated mice to SpDNV (+) surgery or sham SpDNV (−) surgery. We noted that DIO sham-operated mice that underwent SpDNV (i.e., sham + SpDNV) lost weight relative to regular sham mice (Figure 4A), suggesting an important role of the splanchnic nerve in body weight regulation and energy homeostasis. Surprisingly, RYGB mice that underwent SpDNV (i.e., RYGB + SpDNV) started regaining weight by week 2 post-surgery instead of losing or maintaining their body weight. By post-operative week 5, the body weights of both groups (sham + SpDNV and RYGB + SpDNV) seemed to overlap (Figure 4A). The average change in body weight over 5 weeks was −0.442 ± 0.042 g/day in the RYGB group and −0.004 ± 0.022 g/day in the sham group, which regained its pre-operative weight ($p < 0.001$). By contrast, the RYGB + SpDNV (−0.319 ± 0.041 g/day) and sham + SpDNV (−0.238 ± 0.037 g/day) groups had similar overall body weight changes by that time frame (Figure 4B). The selective SpDNV decreased the average daily food intake of sham controls, but not RYGB mice (Figure 4C), which likely accounts for the loss of total body weight and fat mass in this group (Figure 4E). SpDNV also eliminated the RYGB-evoked decrease in feeding efficiency (i.e., amount of weight gain relative to the energy consumed; Figure 4D), increase in total energy expenditure (Figures 4F and 4G), increase in O_2 consumption (Figure 4H), decrease in respiratory exchange ratio (RER) (Figure 4I), and improvement in glucose homeostasis (Figures 4J and 4K). In addition, SpDNV abolishes the RYGB-induced increase in markers of sympathetic nerve activity within the gut (Figures 5A–5C) as well as markers of thermogenesis within vWAT (Figure 5D). Moreover, the increase in TH within vWAT after RYGB was highly localized to UCP1-expressing cells, and this effect is also lost after SpDNV (Figure 5E). Finally, the previously reported shift in phyla within the gut microbiota post-RYGB (Liou et al., 2013) (i.e., decrease in Firmicutes and increase in *Bacteroides*), which was also present in our control surgery group, was lost after selective SpDNV (Figure S6).

The possibility that surgical injury of the intestine or mesenteric fat could have contributed to an inflammation-mediated “browning” within vWAT post-RYGB is unlikely given the lack of any significant infiltration of any inflammatory cell type—neutrophilic or lymphocytic—within vWAT or jejuna of DIO mice 6 weeks after RYGB (Figures S7A and S7B). We also show that circulating levels of tumor necrosis factor alpha (TNF-α) and *Tnfα*

mRNA expression within vWAT, gonadal WAT (gWAT), and jejunum were all similar between sham- and RYGB-operated mice (Figures S7C and S7D). In addition, to show that our surgical interventions did not induce a stress-mediated response, we confirmed that selective SpDNV did not affect the sympathetic nerve activity of the adrenal glands nor the level of circulating catecholamines (Figure S5E). We also show that RYGB surgery itself does not affect the level of circulating catecholamines (Figure S7E).

CB1 Mediates the RYGB-Specific Metabolic Effects on the Gut

To further explore the molecular mechanisms that underlie RYGB-specific splanchnic sympathetic nerve activation and induction of vWAT "browning," we examined several potential signaling pathways in DIO mice after RYGB or SG. Glucagon-like peptide-1 (GLP-1) is secreted from the enteroendocrine L-cells of the intestines in response to digested nutrients. In addition to its known incretin action, it was reported that GLP-1 has a thermogenic effect on vWAT and BAT (Drucker, 2007; López et al., 2015). However, serum GLP-1 is increased after both RYGB and SG (Stefater et al., 2012). It was previously shown that GLP-1 is dispensable for SG and RYGB to induce their weight and glucose regulatory effects (Chambers et al., 2013; Mokadem et al., 2013). Leptin is a peptide secreted from adipocytes and stomach (Cammisotto and Bendayan, 2012) that regulates energy balance by controlling food intake and energy expenditure (Farooqi and O'Rahilly, 2009; Zhang et al., 1994). However, serum leptin levels decreased after both RYGB (Figure S1H) and SG (Figure S2E), and leptin-deficient *ob/ob* mice can still respond to weight regulatory effects of RYGB (Mokadem et al., 2015). Recently, bile acids have emerged as key signaling molecules in the regulation of energy balance in addition to their known role in lipid absorption and cholesterol metabolism (Staels and Fonseca, 2009). They act as ligands for G-protein-coupled receptor (GPCR) and farnesoid X receptor α (FXR-α) to activate thyroid hormones and increase energy expenditure among other functions (Watanabe et al., 2006, 2011; Worthmann et al., 2017). Although FXR was found to be important for energy-regulating effects of SG (Ryan et al., 2014), an increase in circulating bile acids is observed after both RYGB and SG (Figure S7F) (Penney et al., 2015). Finally, peptide YY (P-YY) is a gut-secreted hormone related biochemically to neuropeptide Y (NPY) and has been shown to have an energy-regulating effect mainly by affecting food intake and possibly energy expenditure (Murphy and Bloom, 2006). However, post-prandial total P-YY serum levels were found to be similarly increased after both RYGB and SG surgeries (Figure S7G).

Endocannabinoids, which were originally recognized as primarily central neuromodulators, have multiple physiologic roles (central and peripheral) including energy balance regulation (Lipina et al., 2013; Zou and Kumar, 2018). Endocannabinoid receptor-1 (CB1) signaling can activate autonomic sympathetic neurons, increase energy expenditure, and regulate food and dietary fat intake (Cardinal et al., 2014; DiPatrizio et al., 2011, 2013; Quarta et al., 2010). It was also proposed that CB1 signaling can control gut-microbiota-mediated endotoxemia by regulating "tight junctions" (Alhamoruni et al., 2012) and may alter gut microbiota composition (Mehrpouya-Bahrami et al., 2017), suggesting a dynamic interplay between the two. Examination of DIO mice that underwent bariatric surgery revealed no significant change in *Cb1* mRNA and protein expression in the hypothalamus (Figures 6A and 6B). However, level of *Cb1* mRNA and protein expression were decreased in the Roux

limb (jejunum) of RYGB-, but not SG-operated, mice (Figures 6A and 6B). Three-week treatment of DIO mice with rimonabant (SR141716A), a CB1 inverse agonist, caused a reduction in food intake that lasted for about a week (Figure 6C). The weight-reducing action of SR141716A lasted for up to 18 days (Figure 6D). A PF experiment showed that the anorectic effect of SR141716A does not entirely explain the weight loss evoked by such treatment (Figure 6D), indicating that increase in energy expenditure may have contributed to its weight-reducing effects. Consistent with such possibility, a decrease in feeding efficiency, indicative of increased energy expenditure, was noted in the DIO mice treated with SR141716A (Figure 6E). Furthermore, *Adbr3* and *Ucp1* mRNA expression was significantly increased within vWAT of SR141716A-treated DIO mice compared with PF-placebo (Figure 6F), and TH expression was significantly increased in vWAT and jejunum of SR141176A-treated mice compared with their sham counterparts (Figures 6G and 6H). Administration of SR141716A induces a remarkable increase in the activity of the efferent (i.e., sympathetic) splanchnic nerve fibers compared with placebo-treated shams and PF sham mice (Figures 6I and 6J).

Interestingly, SR141716A-induced weight loss in DIO sham mice was significantly attenuated in SpDNV-operated mice (Figure 7A). Furthermore, the anorectic effect of SR141716A was significantly diminished in the SpDNV group (Figure 7B). We then treated RYGB-operated mice and sham controls with arachidonoylethanolamide (AEA), a potent non-selective CB1 receptor agonist, for 15 days starting 3 weeks after recovery from surgery. The RYGB-AEA group gained more weight than the RYGB-placebo, while the sham-treated groups showed no significant difference (Figure 7C). There was no significant effect of AEA on food intake, but the RYGB-induced reduction in feeding efficiency was lost in the AEA-treated group (Figure 7D). The increase in expression of *Adrb3* in the jejunum and *Ucp1* in the vWAT of RYGB-operated mice was similarly abolished by AEA treatment (Figure 7E).

Together, these findings suggest that RYGB, but not SG, increases total energy expenditure, specifically RMR, by downregulating intestinal CB1 expression, leading to activation of the splanchnic sympathetic nerve traffic to induce browning of vWAT.

DISCUSSION

Bariatric surgery is one of the most effective and long-lasting therapies for management of obesity. RYGB and SG are the two most commonly performed bariatric procedures throughout the world (Buchwald and Oien, 2013). Some studies, however, suggested that RYGB has several advantages over SG in long-term weight maintenance (Maciejewski et al., 2016; Puzziferri et al., 2014). The intestinal rearrangement represents the main anatomical difference between RYGB and SG. Several rodent studies have previously showed, using calculation methods or indirect calorimetry, that RYGB prompts an increase in total energy expenditure (Hao et al., 2017; Mokadem et al., 2013, 2015; Seeley et al., 2015; Stefater et al., 2012). Using both direct and indirect calorimetry, we showed that only RYGB (and not SG) increases anaerobic RMR, which accounts for ~7% of total RMR. Interestingly, this contribution of anaerobic components to the total RMR is similar to what is observed in normal lean animals on regular chow (Burnett and Grobe, 2013, 2014). Similarly, two previous studies in humans showed that anaerobic resting metabolism constitutes ~10% of

the total RMR in lean men and women, an effect that is lost in obese women (Pittet et al., 1974, 1976). It was previously suggested that the human biomass can reach up to 3% of the host's body weight and up to 22% of its caloric turnover (Riedl et. al 2017). Furthermore, it was previously demonstrated that the weight-promoting effects of risperidone (a commonly prescribed antipsychotic medication) are transferable to other animals through gut microbiome and/or its products (Bahr et al., 2015). Remarkably, the recipients of bacteria from risperidone-treated mice exhibited significant reduction in RMR that was predominantly anaerobic RMR. Therefore, we believe that the increase in anaerobic RMR following RYGB is likely from the rearranged microbiome environment induced by this bariatric procedure. Thus, we propose that the "benefit" of anaerobic RMR to a bariatric surgery patient stems from the increased energy output by the subject, which would contribute to weight loss and/or resistance to weight regain even if traditional respirometry-based methods cannot measure it. We and others have therefore argued that respirometry-based estimates of heat production represent an index of "aerobic" metabolism because of this method's myopic focus on oxygen-based metabolism. On the other hand, direct calorimetry-based measurements of heat dissipation represent a measure of "total" metabolism because it is not biased toward any fuel type; therefore, it should be considered —whenever available—in evaluating delicate and dynamic energy balance conditions in combination with respirometry.

We also show that "browning" within vWAT is a key source of this increase in energy dissipation, and it is specific to RYGB. Moreover, we demonstrate that RYGB-induced vWAT "browning" is mediated through increase in splanchnic sympathetic nerve activity and that selective SpDNV of the luminal gut abolishes all the metabolic and energy-regulating benefits of RYGB surgery. Strikingly, RYGB-induced increase in sympathetic tone is specific to the luminal gut, as TH expression was upregulated in the jejuna and vWAT of bypass-treated animals but unchanged in BAT and downregulated in the pancreas. Thus, this process seems selectively programmed to control body weight and glucose homeostasis independently. Remarkably, SpDNV in sham-operated DIO animals induced a weight loss that was sustained for several weeks after surgery and was associated with reduction in daily food consumption (Figures 4A–4C). Although the visceral/afferent fibers that travel along the motor/efferent sympathetic fibers within the splanchnic nerve are similar in nature to the afferents of the vagus nerve, their role and functionality in energy signal communication have not been elucidated independently. Therefore, the neural afferent fibers within either the splanchnic or the vagus nerve could have an important role in communicating key energy signals from the gut to the brain. It was also previously shown that RYGB causes some dystrophic changes of vagal axons within sections of the gastric wall and around the surgical anastomosis, but it does not alter vagal innervation of the rest of the intestines (Gautron et al., 2013).

Interestingly, adding vagotomy to RYGB did not affect weight loss outcome over a 5-year period in more than 1,200 human subjects (Okafor et al., 2015). Also, selective celiac branch vagotomy minimally affected weight loss in rats post-RYGB. Vagotomized rats that underwent RYGB still experienced a relative increase in their food intake compared with non-vagotomized RYGB rats; however, that effect was transient. The overall weight loss difference between the two groups was minimal (Hao et al., 2014). It is, however, intriguing

that the loss of a large and crucial nerve such as the vagus had minimal consequences on the metabolic effects of RYGB, whereas the loss of the splanchnic had such dramatic effects. Future investigations are needed to understand the functional difference between the afferents of the splanchnic versus the vagus nerve regarding energy regulation along the gut-brain axis. Another possible explanation of the energy phenotype post-RYGB may involve the interrupted enteric nervous system of the gut after surgery. The newly rearranged intrinsic neuronal network post-surgery could potentially modulate luminal energy signals that are being transmitted along the gut-brain axis through the afferent fibers of the autonomic nerves.

We also showed that *CB1* expression within the small intestine is downregulated post-RYGB, but not SG, and that administration of a CB1 inverse agonist to DIO mice can mimic the effects of RYGB on energy expenditure. Conversely, administration of CB1 agonist significantly attenuates the weight loss and energy-regulating effects of RYGB. Our findings suggest that the gut luminal environment post-RYGB arrangement leads to decrease in intestinal (i.e., peripheral), but not hypothalamic (i.e., central), CB1 expression. This selective alteration in CB1 expression constitutes a new energy signal that is relayed—via the afferent sensory fibers of the splanchnic nerve—to the central nervous system where it is interpreted and subsequently activates sympathetic motor neurons, leading to an increase in activity of the efferent fibers of the splanchnic nerves, which activate “browning” within vWAT. This proposed mechanism is further supported by the observation that SpDNV itself causes weight loss that is mainly driven by food intake reduction, suggesting a role of the sensory afferent fibers of the splanchnic nerves in regulation of energy intake. Moreover, administration of CB1 inverse agonist rimonabant causes an initial transient reduction in food intake in addition to an increase in energy expenditure and vWAT thermogenesis. This anorectic effect of rimonabant was significantly mitigated after splanchnic denervation, again suggesting that intestinal CB1 is a key regulator of afferent energy signals along the gut-brain axis. Furthermore, Gómez et al. (2002) showed that a peripheral mechanism of CB1 receptor can modulate feeding behavior via the sensory vagal afferent fibers. It would have been interesting to measure the endogenous cannabinoid levels—AEA and 2-arachidonoyl glycerol (2-AG)—within the intestines, WAT, and hypothalamus of RYGB- and sham-operated mice. However, these lipid-soluble compounds are not easily collected, isolated, and measured, and we, unfortunately, were unable to perform these experiments during the current study.

It should also be noted that previous studies have shown that high-fat diet (HFD) induces an increase in intestinal expression of CB1 as well as tissue and plasma cannabinoids in mice (Argueta and DiPatrizio, 2017). On the other hand, inhibition of peripheral CB1 signaling attenuates obesity and reverses the HFD-induced changes in intestinal CB1 expression (Argueta and DiPatrizio, 2017). Furthermore, human subjects who received taranabant, an acyclic CB1 inverse agonist, lost more weight than would be expected by reduction in food intake alone, suggesting an increase in energy expenditure after CB1 blockade (Addy et al., 2008). Although cannabis (marijuana) is the most commonly used recreational drug in the US, and its use among young people has been increasing since 2007 (Han et al., 2019), there are no data on the effects of cannabis use after weight loss induced by surgery. Previous studies showed a greater lifetime prevalence of all substance abuse/dependence in the

bariatric population than in the general population, with a reported rate of 14.6% (Heinberg et al., 2010). One study demonstrated that marijuana use significantly increased the rate of disordered and unhealthy eating behavior after bariatric surgery (Sarwer et al., 2004), and loss of control over eating behavior has been shown to be a strong predictive factor for weight regain after bariatric surgery (Conceição et al., 2014; Odom et al., 2010). Therefore, weight regain in a subset of individuals with a history of gastric bypass could be due to cannabis use and might be otherwise preventable.

Gastric bypass was previously shown to induce a conserved shift in the composition of gut microbiota that, when transferred to germ-free mice, can induce similar metabolic and weight regulatory effects to those of the donors (Liou et al., 2013; Tremaroli et al., 2015). We did show—as did the previous studies mentioned above—that RYGB increases the ratio of *Bacteroidetes*/Firmicutes as well as a distinctive increase in the abundance of Proteobacteria phylum (Figure S6A). Proteobacteria was also shown to be positively associated with “browning” of adipose tissue (Moreno-Navarrete et al., 2018). Remarkably, the ability of RYGB to increase abundance of the Proteobacteria phylum was lost after selective SpDNV, which also resulted in multiple other microbial alterations at the genus level (Figures S6A and S6B).

The discrepancy in the mechanisms involved in RYGB versus SG is further supported by a previous study showing that RYGB, but not SG, activates specific pathways along the gut-brain axis, specifically the nucleus tract solitarius and the dorsal motor nucleus of the vagus (Ballsmider et al., 2015). Furthermore, at the anatomical level, RYGB significantly differs from SG by the way it affects the gut’s autonomic neuronal assembly. The ventral and dorsal gastric branches of the vagus nerve are usually transected during pouch formation of the RYGB surgery, disturbing vagal innervation of the excluded stomach, but not the pouch or the distal intestines (Figure S7H). However, only distal axonal injuries of both ventral and dorsal gastric branches of the vagus occur post-SG, while a significant portion of the splanchnic nerve traveling along the greater gastric curvature is resected and no further rearrangement occurs after SG (Figure S7I). On the other hand, splanchnic innervation, which follows the vascular supply of the gut, is minimally damaged post-RYGB and gets radically rearranged due to the new connection of the jejunum to the gastric pouch (Figure S7H).

Our findings point to the splanchnic nerve subserving the gut as a key player in energy homeostasis and in underlying the beneficial metabolic effects of RYGB. Reduction in food intake is a very important factor in energy balance post-RYGB in humans (compared with studies on rodents), but the contribution of RMR increase (or an attenuated decrease in RMR compared with pre-operative values) is still controversial (Thivel et al., 2013). Another finding in our study relates to the identification of the significance of a non-anaerobic component of the RMR, which can only be measured using a combination of direct and indirect calorimetry. This could explain the failure to detect an increase in total energy expenditure or RMR in humans who underwent RYGB since most of the studies used only indirect calorimetry (Thivel et al., 2013). Another caveat that could also contribute to bias in interpreting respirometry data in humans is the high prevalence of dumping syndrome post-RYGB, which was reported to be ~40% of all patients (van Beek et al., 2017). Consistent

with our findings, a study that measured RMR changes (using respirometry or indirect calorimetry) in women who underwent bariatric surgery compared with subjects with equivalent low caloric diet found that the bariatric-operated subjects had similar “decrease” in RMR at 8 weeks, yet they lost almost twice as much weight as the control group (Tam et al., 2016). This suggests that the surgery-operated group had another energy expenditure component that was not accounted for by the method used for measurement of RMR (i.e., the indirect calorimetry).

In summary, our findings highlight a role of CB1 and the splanchnic sympathetic nerves in mediating the energy homeostatic effects of gastric bypass. These findings might open future opportunities to develop new targets for management of obesity at the molecular and/or physiologic levels. Rimonabant previously failed the challenge test as a potential drug therapy for obesity, mainly because of its neuro-psychiatric side effects (Sam et al., 2011). Nonetheless, the above-mentioned findings suggest an intriguing role of peripheral CB1 in food intake regulation, independent of its central counterpart. Therefore, a better understanding of the signaling pathways underlying the endocannabinoid-system-mediated regulation of energy balance could possibly lead to a targeted pharmacotherapy for treatment of obesity.

We showed that RYGB induces increase in splanchnic nerve activity that drives its metabolic effects (through its efferent motor branch), while we also showed that SpDNV induces weight loss mainly by decreasing food intake (likely by modulating afferent sensory signals) and relative improvement in glucose metabolic measures. It should be noted, however, that the improvement in glucose and insulin tolerance tests post-SpDNV could be due to the weight loss per se or possibly due to hepatic sympathetic denervation and its resulting changes in glucose metabolism. Irrespective of the mechanism involved, our findings could open opportunities to manipulate the splanchnic nerves or some of their branches to develop new therapeutic options for the treatment of obesity and type 2 diabetes. A US patent to develop a splanchnic nerve stimulator for treatment of obesity was filed in 2002, but it was unsuccessful in leading to a usable device for that purpose (US patent US20120053660A1). However, these results uncover the importance of splanchnic nerves as significant regulators of energy balance at multiple levels (sensory and motor). Therefore, future studies dedicated to examining the specific role of the afferent fibers of the splanchnic nerves in communicating energy signals across the gut-brain axis would be of paramount importance.

STAR★METHODS

RESOURCE AVAILABILITY

Lead Contact—Further information and requests for resources and reagents should be directed to and will be fulfilled by the Lead Contact Mohamad Mokadem (mohamad-mokadem@uiowa.edu).

Materials Availability—This study did not generate new unique reagents.

Data and Code Availability—The datasets generated and analyzed during the study are included with the published manuscript (and Supplemental Information). The microbiota 16

s sequencing analysis data are available to public at the following link: https://www.ncbi.nlm.nih.gov/bioproject/ PRJNA630080 under the name “Roux-en--Y Gastric Bypass (RYGB) and Sham dataset” with the corresponding SRA accession code: PRJNA630080. All other data are available from the corresponding author upon request.

EXPERIMENTAL MODEL AND SUBJECT DETAILS

RYGB Human Subjects—Control subjects (3 females and 1 male, ages from 38 to 65 years old) were obese patient candidates who underwent RYGB at the Paris Diderot University hospital and a sample from the jejunum (close to the site of the planned gastro-jejunal anastomosis) was collected at the time of the surgery. RYGB subjects (5 females, ages from 32 to 56 years old) were obese patients who underwent gastric bypass surgery (at least 1 year prior to sample collection) and had an adequate weight loss response but had to undergo reoperation due to complications such as persistent ulcers, dumping syndrome, or under nutrition (Table S1). Samples of jejunum 5 cm from the anastomosis are routinely taken when bypass-operated patients underwent reoperation due to such complications. All patients were consented for sample collection of tissues before the operation and an institutional review board (IRB) permission was obtained to access the tissue collected and perform the appropriate staining described in the supplementary material.

SG Human Subjects—Subjects were obese patients who underwent SG at University of Iowa Hospitals and Clinics for morbid obesity, had adequate weight loss response but needed to undergo another surgery or endoscopic procedure for reasons such as: dilated fundic remnant, refractory dysphagia, diarrhea or reflux symptoms. Only patients (2 males and 3 females, ages from 37–55 years old) who had tissues collected at the two time points (during SG operation and on follow-up procedure) were included. All secondary procedures occurred 1–5 years after the initial surgery where a gastric sample was obtained (Table S2). All patients were consented for sample collection of tissues before the operation. In addition, an institutional review board (IRB) permission was obtained to access the tissue collected and perform the appropriate staining described in the supplementary material.

Primates—Adult Rhesus Macaques 14 males (9–12 years old) were single housed indoors in the Oregon National Primate Research Center (ONPRC). Animals were fed a western style diet (TAD Diet 5L0P; Research Diets, 36% calories from fat) to induce obesity. (Note: the normal Macaques diet contains ~15% calories from fat). TAD diet was provided *ad libitum* twice daily and food intake was monitored during both meals. The group was then divided into an RYGB arm and a Sham surgery arm. All surgeries were performed by surgical veterinarians from the division of comparative Medicine at ONPRC. All animal care and procedures were reviewed and performed according to the ONPRC Institutional Animal Care and Use Committee at Oregon Health and Science University.

Mice—Care of all animals and procedures were approved by the Animal Care and Use Committees at the University of Iowa (protocol number 4101186), the University of Texas Southwestern Medical Center. Male DIO C57BL/6J mice were purchased from Jackson Laboratories (strain number 380050) at the age of 16–17 weeks. Male lean C57BL/6J mice were purchased from Jackson Laboratories (strain number 000664) at the age of 6–7 weeks.

Upon arriving, mice were continued on the same high fat diet (Research Diets, D12492) for DIO mice and normal diet (Teklad 7913) for lean mice and maintained on a 12-hr light-dark cycle. Water and food were available *ad libitum* except when mice were fasted as described below.

METHOD DETAILS

RYGB and SG Surgeries in Mice—All animals were given a weight-based dose of antibiotics (enrofloxacin) as prophylaxis for peri-operative infection and analgesics (buprenorphine) for pain management before laparotomy. The surgical rearrangement of Roux-en-Y anatomy and their sham controls were performed as described in our previous studies (Hao et al., 2017; Zechner et al., 2013). The same prophylactic treatment with antibiotics and analgesics were also received by SG-operated mice and their sham controls. The abdomen was sterile, prepped by removing hair with an electric razor, three steps of scrubbing with betadine, and wiping with alcohol. Midline laparotomy was performed using forceps and scissors and extended from the xiphoid to umbilicus. The abdominal wall was entered using forceps and sterile cotton swabs. The stomach was exposed and transected to form a tubal sleeve. The sleeve portion of the stomach was closed, and the greater curvature portion removed. The stomach sleeve was then placed back *in situ*. Closure was performed using 4−0 Vicryl (or PDS) with a running suture in the abdominal wall and interrupted sutures using 4−0 nylon + Vetbond Tissue adhesive glue in the skin. In the sham procedures, the abdomen was opened in the same manner and a clip applicator was applied with gentle pressure to the outside of the stomach for several minutes along the line of resection of the sleeve. The bowels were manipulated without any rearrangement until the anesthesia time matched that of the actual surgery. Abdominal wall and skin closures were performed in the same manner. Different segments of small intestinal tissues are collected systematically in all our operated mice as follows: We measure anatomically 6 cm from the pylorus and then cut to harvest the Biliopancreatic limb or duodenum. We measure 4 cm from the ligament of Treitz and then cut to create the Roux limb. We collect 6 cm from that point forward and call it Roux limb or jejunum. Finally, we collect the distal 6 cm of the ileum before it connects to the cecum.

Study Design and Surgery—Several groups of 18- to 19-week-old diet-induced obese mice with appropriate body weight (40–45 g) underwent RYGB versus RYGB-sham surgery or SG versus SG-sham surgery. All mice recovered from stress of surgery in their home cages, with daily prophylactic injection of analgesics for the first 2 days and then on as-needed basis. They were also placed on liquid diet and supplemental intra-peritoneal injections of dextrose fluid for hydration and nutrition during postoperative week 1. They were all allowed to recover on solid diet during postoperative week 2. Experiments were performed between postoperative weeks 2 and 6 with the exception of one splanchnic nerve electrical activity recording that was performed between post-operative week 1 and 2. Separate groups underwent separate experiments. One group was dedicated for measurement of food intake, stool calorie loss, energy efficiency, and body composition. Another group was dedicated for measurement of total energy expenditure by the CLAMS as well as glucose and insulin tolerance tests. One group was generated for surface body temperature assessment by an infrared camera. Finally, separate groups were generated for each

sympathetic nerve activity reading. One group of 8-week-old lean C57BL/6J mice (strain number 000664, Diet: Teklad 7913) underwent the selective splanchnic denervation experiment.

Splanchnic and BAT Sympathetic Nerve Activity (SNA) Recordings—After recovery from sham or RYGB surgery (during post-operative week 1 or 6), mice were anesthetized with intraperitoneal administration of ketamine (91 mg/kg body weight) and xylazine (9.1 mg/kg body weight). Intubation with PE-50 was performed to provide an unimpeded airway for spontaneously breathing of O_2 enriched room air. Micro-renathane tubing (MRE-40, Braintree Scientific, Braintree, MA) was inserted into the right jugular vein for infusion of the anesthetic agent α-chloralose (initial dose 12 mg/kg, sustaining dose 6 mg/kg/hr). Another MRE-40 tubing was inserted into the left carotid artery for continuous measurement of arterial pressure and heart rate. Core body temperature was maintained at 37.5°C with the use of a heated surgical table. A left retroperitoneal incision was made to access the bilateral greater splanchnic nerve fibers connecting the cardiac ganglia to the celiac ganglia. To record BAT SNA, an incision was made on the dorsal surface to expose the BAT in the nape of the neck. An intact unilateral multi-fiber splanchnic or BAT nerve bundle was carefully isolated and placed on a bipolar platinum-iridium wire (36-gauge, A-M Systems, Sequim, WA) and sealed with silicone gel (Kwik-Sil, World Precision Instruments, Sarasota, FL). The nerve recording electrode was attached to a high impedance probe (HIP511, Grass Instruments, West Warwick, RI) leading to an AC preamplifier (P5, Grass Instruments) that magnified the nerve signal at 10^5 power with a low and high frequency filter cutoff at 100 and 1Khz, respectively. The signal from the nerve was routed to a data acquisition system (MacLab Model 8 s), which counted the number of nerve spikes that exceeded a threshold level set just above the noise level each second (spikes/sec) and to a resetting voltage integrator (RVI: Model B600c, University of Iowa Bioengineering) that measures the total voltage. After allowing all hemodynamic parameters to stabilize, a basal recording of SNA was continuously monitored for the next 30 minutes. At the end of the study, the mouse was euthanized, and residual background noise was excluded in the assessment of SNA by correcting for post-mortem activity.

Intact and Efferent Splanchnic SNA—A separate cohort of mice was anesthetized and prepared with a trachea tube, arterial/venous cannulations and splanchnic SNA recording as above. At the end of the 30-minute basal measurement of splanchnic SNA, the study was extended by surgically sectioning the same splanchnic nerve fibers caudal to the site of the recording electrode. The recording of the central end of the unilateral efferent splanchnic SNA (e-SpSNA) was measured for the next 60 minutes. At the end of the study, the mouse was euthanized, and residual background noise was measured and excluded in the assessment of intact and e-SpSNA by correcting for post-mortem activity.

Bilateral Splanchnic Denervation with Celiac Ganglionectomy—Mice were anesthetized with isoflurane (5% induction, 1%–2% sustaining). An abdominal incision was made, and all visceral organs were gently moved to expose the abdominal aorta, vena cava, and nearby connective tissue in the area between the cardiac and celiac ganglions. Embedded in the connective tissue, bilateral sympathetic chains of the greater splanchnic

nerves were first identified and then tracked caudally, until they merged into the celiac ganglion. A 0.5–1 mm segment from both chains of the splanchnic sympathetic nerves was sectioned. Next, the celiac ganglion was carefully stripped free from the nearby aorta, vena cava, and connective tissue. A solution of phenol (10% phenol in 70% ethanol) was used to paint the region where the celiac ganglion was located to deaden any residual nerve fibers. Upon completion of the splanchnic nerve denervation and celiac ganglionectomy, all visceral organs were allowed to return to their original position. The abdomen was closed as described above. RYGB and sham mice were immediately prepared for surgery.

Measurement of Total Energy Expenditure using Indirect Calorimetry—Food intake, activity, and energy expenditure were all determined through the use of specially-designed chambers within the University of Iowa Metabolic Phenotyping Core Facility using the CLAMs system which relies on indirect calorimetry (respirometry) for energy assessment between post-operative week 2 and 3. Animals were individually housed for 5 days in standard housing preceding placement into metabolic chambers for acclimatization. They were then moved into free-running cages with 24-hour access to food and water. Data were continuously recorded 24 hours per day, and daily welfare checks were manually performed. Circadian food intake, O_2 consumption, CO_2 production and locomotor activity were continuously measured during this time period.

Measurement of Resting Metabolic Rate using Direct Calorimetry—Resting metabolic rate was measured using a custom-made chamber of combined direct and indirect calorimetry system for single mouse measurements over maximum 10-hour period while accounting for activity and sleeping times. This device was previously demonstrated to be superior to respirometry in accurately assessing the total resting metabolic rate in mice (Burnett and Grobe, 2013; Walsberg and Hoffman, 2005).

Feeding efficiency—Feeding efficiency is calculated and refers to the rate of body mass gain per amount (mass, or caloric content) of food ingested by an animal.

Surface Body Temperature Measurement by Infrared Camera Recorder—The surface body temperature of RYGB and sham-operated mice was recorded during postoperative week 3 using a high-resolution infrared camera (A655sc Thermal Imager; FLIR Systems, Wilsonville, OR). Quantitative analysis of infrared images was performed using FLIR Research IR software version 3.4.13039.1003. Mice were imaged on a multilane treadmill next to their age-matched littermate controls at baseline and after 6 minutes of treadmill exercise at 7 m/min and 15° incline. Images were obtained every 1 s. The side-by-side imaging of mice in the same camera frame allows simultaneous assessment and direct comparison of the body surface heating in the different mouse models, providing an advantage over other methods for assessing body temperature that would be limited by the accuracy and concordance of two separate temperature probes. Surface temperature recordings were obtained first in the midst of the light cycle (sleeping or fasting cycle) and were repeated later in the week during the midst of the dark cycle (awake or feeding cycle).

FDG uptake study by PET scan—FDG studies were conducted at the University of Texas Southwestern Medical Center. C57BL/6J purchased from Jackson Laboratory were

housed in thermoneutral conditions (29°C, 12 hours light/dark cycle) and fed a 60% fat diet (Research Diets, D12492) as described above. After 12 weeks of HFD feeding, PET-CT imaging was performed in the Small Animal Imaging facility. Briefly, mice were removed from their home cages and fasted overnight before the scan. Ten minutes prior to imaging, mice were anesthetized using 3% isoflurane at room temperature until stable vital signs were established. Mice were then placed onto the imaging bed under 2% isoflurane anesthesia for the duration of imaging. The CT image was acquired at 80 kV and 500 μA, focal spot of 58 μm. After the CT scan, the mouse was injected intravenously with ~37 MBq (100 μCi) of FDG and a 0–60 min dynamic PET was immediately performed. Reconstructed CT and PET images were fused and analyzed using ORS Visual software. One week later, mice underwent either RYGB or sham surgery as mentioned above. Mice were maintained on a post-operative feeding protocol during which liquid diet was provided from post-operative days two through seven. On post-operative day 6, 0.25 g of HFD was provided on a daily basis until consumed in its entirety. After surgical recovery, RYGB mice were given *ad libitum* access to HFD, while weight-matched sham mice were provided HFD once a day at the onset of the dark phase. The amount of food given to the weight-matched-sham group was adjusted to induce weight loss equal to that of the RYGB group. Four weeks after the surgeries, both groups of mice underwent a second round of FDG injections and FDG-PET/CT scanning.

CB1 Inverse agonist Rimonabant (SR 141716A) Experiment—DIO male C57BL/6J mice were purchased from Jackson Laboratories (strain number 380050) at the age of 16 weeks. One week after single housed, Rimonabant (SR 141716A) (Cat# 0923, Tocris Bioscience; Cat# 0800–25 mg, Sigma) was administered to one group of the DIO mice prepared in 0.2% tween-80 for 18 days (10 mg/Kg/daily) by oral gavage. Control (placebo) and pair-fed to SR 141716A (PF-placebo) controls were treated with 0.2% tween-80 by daily oral gavage. Another group of DIO mice underwent splanchnic denervation or Sham surgery. After recovery for 9 days, the mice were gavaged with placebo or 10 mg/Kg SR 141716A daily for 12 days. The splanchnic SNA was measured in sham group before sacrifice. Food intake, feeding efficacy and body mass were measured as described above. Mice were gavaged with 10 mg/Kg SR 141716A or placebo 45 mins before sacrifice.

CB1 agonist Arachidonylethanolamide (AEA) Experiment—After 3 weeks recovery from RYGB or Sham surgery, mice were treated with AEA (Cat# A0589–25mg, Sigma) prepared in sunflower oil for 16 days (20 mg/Kg/daily) or vehicle (sunflower oil) by oral gavage. We decided on the above-mentioned dose based on previous report by Aguirre et al., 2015 (2017) showing that it can affect body weight, body fat mass, and peripheral CB1 expression irrespective or food intake. Body weight, food intake and feeding efficacy (calculated as described above) were recorded accordingly. Mice were treated with AEA (20 mg/Kg) or vehicle 45 mins before sacrifice and tissue was collected afterward for analysis.

Glucose Tolerance Test—Following an overnight fasting (6:00 pm to 10:00 am) during post-surgery week 4–5, mice were administered 1g/kg body weight of D-Glucose (Cas No: 50–99-7, RPI, Mt. Prospect, IL) by oral gavage. Blood glucose was measured from tail vein

blood using a hand-held glucometer (Contour, Bayer HealthCare LLC, Mishawaka, IN,46544) immediately before and 15, 30, 60, 90 and 120 minutes after glucose administration.

Insulin Tolerance Test—Following a 4-hour fast (9:00 am to 1:00 pm) during postoperative week 5 or 6, mice were administered 0.75 U/kg body weight dosage of insulin (NDC 0002–8215-01, HI-210, Humulin R, Eli Lily) by intraperitoneal injection. Blood glucose was measured from tail vein blood using a hand-held glucometer (Contour, Bayer HealthCare LLC, Mishawaka, IN,46544) immediately before and 15, 30, 60, 90 and 120 minutes after insulin administration.

Immunohistochemistry Staining of TH in Human Samples—Tyrosine hydroxylase (TH) immunohistochemistry was performed on 4-μm-thick tissue sections after deparaffinization, rehydration, and PT Link (Agilent Dako; Santa Clara, CA) heat-induced epitope retrieval in HpH Target Retrieval Solution (Agilent Dako; pH 9) on an Autostainer Link 48 (Agilent Dako) using a rabbit monoclonal antibody (2025-THRAB, PhosphSolutions, Aurora, CO, 1:400 dilution; 30 minute incubation) and the polymer-based EnVision+ detection system (Agilent Dako; 15 minute incubation).

Immunohistochemistry Staining of UCP1 in Mouse vWAT—4% paraformaldehyde fixed paraffin embedded vWAT samples were section to 5 μm thickness. After deparaffinize, rehydrate, and antigen-retrieval (10 mM sodium citrate buffer, pH 6.0), sections were blocked in 3.0% hydrogen peroxide in PBS for 8 mins, and the tissues permeabilized with 0.5% Triton X-100 in PBS for 10 mins. Then, tissues were incubated with egg substitute for 15 mins to block endogenous biotin. After 3 times washing, block with 5% fat free milk for 15 mins, after wash, following with 5% horse serum in PBS-T for 30 min at room temperature. Then, sections were incubated with anti-goat UCP1 antibody (sc-6528, 1:150, Santa Cruz) prepared in fresh blocking buffer overnight at 4°C in humidified chamber. The following day, after a brief wash with PBS 3 times, sections were incubated with secondary antibody Donkey anti Goat-Strep biotin (1:500 in 5% horse serum in PBS-T) at room temperature for 30 min. After 3 times PBS washing, applied Streptavidin-HRP (1:500) for 30 mins. After washing with PBS 3 times and ddH_2O twice, applied 100 μl DAB substrate (Dako liquid DAB+ substrate chromogen system, Dako North America) and incubation for 7 min ddH_2O was added to stop the reaction. After counterstain with Hematoxylin, sections were dehydrated and mounted with mounting medium (permamount). Images were visualized under microscopy.

Immunofluorescence and Confocal Microscopy in Mice and Non-Human Primates—4% paraformaldehyde fixed paraffin embedded intestine samples were section to 5 μm thickness. After deparaffinize, rehydrate, and antigen-retrieval (10 mM sodium citrate buffer, pH 6.0), sections were blocked in 5% goat serum in PBS-T (0.3% Triton X-100) for 1 hour at room temperature. Then, sections were incubated with anti-rabbit tyrosine hydroxylase antibody (1:200) with or without anti-goat UCP1 (sc-6528, 1:150, Santa Cruz) and anti-rabbit CGRP (Cat# C8298, 1:500, Sigma) prepared in fresh blocking buffer overnight at 4°C in humidified chamber. The following day, after briefly washing with

PBS three times, sections were incubated with secondary antibody Alexa 488 goat anti-rabbit (1:1000) with or without Alexa 568 donkey anti-goat (1:1000) in 5% goat serum in PBS-T at room temperature for 2 hours. After 3 times PBS washing, sections were mounted with mounting medium with DAPI. Images were visualized using confocal microscopy Zeiss LSM710.

Real-Time Quantitative PCR—To measure thermogenic gene expression, total RNA was isolated from snap-frozen BAT, WAT (visceral mesenteric and subcutaneous), Roux limb (or jejunum), Bilio-Pancreatic (BP) limb and ileum using Direct-zol RNA MiniPrep kit (Zymo Research, Irvine, CA). Total RNA (1 μg) was reverse transcribed to cDNA using cDNA High Capacity Reverse Transcription Kit (Applied Biosystems, Thermo-Fisher). Real-time quantitative PCR (10 ng cNDA, 0.5 μM primers) was performed using iQ™ SYBR® Green (Bio-Rad, Hercules, CA) per manufacturer's instructions. The following primers were used:

β3-ADR Forward	GCC TTC CGTCGT GGT CTT CTG TG
β3-ADR Reverse	GCC ATC AAA CCT GTT GAG C
UCP1 Forward	GGA TGG TGA ACC CGA CAA C
UCP1 Reverse	CTT GGA TCT GAA GGC GGA C
PRDM16 Forward	GTA GCT GCT TCT GGG CTC A
PRDM16 Reverse	CGT CAC CGT CAC TTT TGG CT
CB1 Forward	GGG CAA ATT TCC TTG TAG CAG
CB1 Reverse	CTC AGT CTT TGA TTA GGC CAG G
rps18 Forward	CTG CCA TTA AGG GCG TGG
rps18 reverse	TGA TCA CTC GCT CCA CCT CA

Ribosomal related protein s18 (*Rps18*) mRNA expression was used as an internal control to normalize mRNA expression of these genes.

Western Blot Analysis—Tissues were homogenized in tissue lysis buffer (50 mM HEPES pH7.5, 150 mM NaCl, 1 mM $MgCl_2$, 1 mM $CaCl_2$, 10 mM NaF, 5 mM EDTA, 1% Triton X-100, 2 mM sodium orthovanadate and Roche cocktail protease inhibitor tablet). Protein samples (30 μg) were injected to 8% SDS-PAGE gel or 15% SDS-PAGE gel for CGRP and electro-transferred to a PVDF membrane (Bio-Rad). After blocking with 5% w/v non-fat dry milk in TBST (0.1% Tween 20), each membrane was probed with anti-TH (2025-THRAB, 1:2000, PhosphSolutions, Aurora, CO), CGRP (C-8198, 1:2000, Sigma), CB1 (ab23703, 1:1000, abcam), β-actin (60008–1-Ig, 1:100000, Proteintech) or GAPDH (sc-32233, 1:50000, Santa Cruz) overnight at 4°C, followed with a secondary anti-rabbit or anti-mouse antibody (1:10,000) for TH, CGRP, β-actin or GAPDH respectively, at room temperature for 2 hours. Visualization was performed with an enhanced chemiluminescence (ECL) detection kit (GE Healthcare, Little Chalfont, UK) followed by autoradiography.

Measurement of Stool Calorie Losses—Stool that was collected along with food intake was dried, weighed on a daily basis, and analyzed using bomb calorimetry (University of Arkansas Center of Excellence for Poultry Science, Fayetteville, AR, 72701). To assess

for stool energy loss, total energy output (from stool combustion) was subtracted from total energy intake (from food consumption) and reported as difference in Kcal/day.

Measurement of Serum Leptin—Mice were fasted for 5 hours. Serum was collected in EDTA coated tube and serum leptin was measured using Meso Scale Discovery (MSD) metabolic assays mouse metabolic kit (Catalog No. K15124C-1, from MSD).

Measurement of Serum Total Bile Acids—Mice were fasted for 5 hours. Serum was collected in EDTA coated tube and serum total bile acid was measured using mouse total bile acids kit (80470, Crystal Chem).

Measurement of Serum P-YY—Blood of RYGB, SG and their Sham counterparts was collected (4 hours after meal initiation) in EDTA coated tube and total serum P-YY was measured using Meso Scale Discovery (MSD) U-PLEX Mouse PYY (total) Assay (Catalog No. K1526BK, from MSD).

Measurement of Serum Catecholamine Levels—Serum was collected in EDTA coated tube from lean C57BL/6J mice that underwent the selective splanchnic denervation experiment or Sham/ RYGB operation, and catecholamine concentration (epinephrine (EPI) and norepinephrine (NE)) were measured in Hormone Assay and Analytical Resource Core in Vanderbilt University.

Microbiota Sequencing Analysis—Ceca of mice were snapped frozen in liquid nitrogen and stored at −80°C. Microbial DNA was extracted from cecum using the MoBio PowerSoil Kit (MoBio Laboratories, Carlsbad, CA, USA) as per the manufacturer's instruction with a bead-beating step. Sequencing of the V3–V5 region of the 16 s rRNA was performed at Iowa Institute of Human Genetics (IIHG) using Illumina MySeq platform at Iowa Institute of Human Genetics (IIHG) facility. The raw 16S data were processed by IM-TORNADO to form operational taxonomic units (OTUs) at 97% similarity level (Jeraldo et al., 2014). *Data analysis:* β-diversity (Bray-Curtis and UniFrac distances) measures were calculated based on the rarefied OTU counts. Differential abundance analysis was performed using the Wilcoxon rank-sum test at phyla levels.

QUANTIFICATION AND STATISTICAL ANALYSIS

Data are expressed as means ± SEM and analyzed by Student's t tests or one- or two-way ANOVA, followed by Tukey-Kramer post hoc analysis when ANOVA reached significance. Statistical analyses were performed using Graphpad prism 7.0 (GraphPad software). A $p < 0.05$ was considered statistically significant. ANCOVA was used to correct resting metabolic rate data for body mass using SPSS, as indicated by the term ANCOVA-adjusted RMR which refers to heat production (estimated by respirometric gas exchange) or heat dissipation (measured by direct calorimetry) that is corrected for the covariate of body mass using (univariate) generalized linear modeling. This approach is recommended by field magnates in a recent "Guide to analysis of mouse energy metabolism" manuscript published in Nature Methods (Tschöp et al., 2011). Respirometry-based estimates of heat production represent the "aerobic" RMR measurements because of this method's myopic focus on

oxygen-based metabolism, whereas direct calorimetry-based measurements of heat dissipation represent the “total” RMR because this method is not biased toward any particular fuel type. By extension, “anaerobic” RMR is calculated as “total” minus “aerobic” RMR.

Supplementary Material

Refer to Web version on PubMed Central for supplementary material.

ACKNOWLEDGMENTS

We would like to thank the technical director (Jamie Soto) and staff members of the Metabolic Phenotyping Core facility at the University of Iowa for all the services provided. We would also like to thank Teresa Ruggle for designing our graphic pictures, as well as Kristina Greiner and Paul Casella for their critical review of the manuscript. M.M. is supported by funds from the VA Merit Review Program (I01 BX004774-01), the American Gastroenterological Association Gut Microbiome Pilot Research Program (18185800 BR01), the Department of Internal Medicine at University of Iowa Carver College of Medicine, and the University of Iowa Fraternal Order of Eagles Diabetes Research Center. K.R. is supported by funds from the NIH (HL084207), the American Heart Association (14EIA18860041), and the University of Iowa Fraternal Order of Eagles Diabetes Research Center. D.C. is supported by funds from Cedars-Sinai Institutional Support funds. J.L.G. is supported by funds from NIH (HL134850 and HL084207 to J.L.G.), the MCW CSTI “Obesity” Ensemble (UL1TR001436), the American Heart Association (18EIA33890055 to J.L.G.), and the Advancing a Healthier Wisconsin endowment. M.L.G. is supported by funds from INSERM. L.V.Z. is supported by funds from the NIH (NDK092412) and the VA Merit Review Program (1I0BX000718). L.R.-P. is supported by a PhD program from “Fondation pour la Recherche Médicale” and André Bado by “Fonds d’Aide à la Recherche et à l’Evaluation en hépato-gastroentérologie” (FARE). R.A.R. and C.M.L.B. were supported through an institutional T35 (HL007485). M.A.E.H. is supported by research training funds from the Stead Family Department of Pediatrics at University of Iowa Carver College of Medicine. The Zeiss LSM710 in the University of Iowa’s Central Microscopy Research Facilities used for confocal imaging is funded by the NIH (1 S10 RR025439-01).

REFERENCES

Adams TD, Davidson LE, Litwin SE, Kim J, Kolotkin RL, Nanjee MN, Gutierrez JM, Frogley SJ, Ibele AR, Brinton EA, et al. (2017). Weight and Metabolic Outcomes 12 Years after Gastric Bypass. N. Engl. J. Med. 377, 1143–1155. [PubMed: 28930514]

Addy C, Wright H, Van Laere K, Gantz I, Erondu N, Musser BJ, Lu K, Yuan J, Sanabria-Bohórquez SM, Stoch A, et al. (2008). The acyclic CB1R inverse agonist taranabant mediates weight loss by increasing energy expenditure and decreasing caloric intake. Cell Metab. 7, 68–78. [PubMed: 18177726]

Aguirre CA, Castillo VA, and Llanos MN (2015). The endocannabinoid anandamide during lactation increases body fat content and CB1 receptor levels in mice adipose tissue. Nutr. Diabetes 5, e167. [PubMed: 26098446]

Aguirre C, Castillo V, and Llanos M (2017). Oral Administration of the Endocannabinoid Anandamide during Lactation: Effects on Hypothalamic Cannabinoid Type 1 Receptor and Food Intake in Adult Mice. J. Nutr. Metab. 2017, 2945010. [PubMed: 28808587]

Alhamoruni A, Wright KL, Larvin M, and O’Sullivan SE (2012). Cannabinoids mediate opposing effects on inflammation-induced intestinal permeability. Br. J. Pharmacol. 165, 2598–2610. [PubMed: 21745190]

Argueta DA, and DiPatrizio NV (2017). Peripheral endocannabinoid signaling controls hyperphagia in western diet-induced obesity. Physiol. Behav. 171, 32–39. [PubMed: 28065722]

Bahr SM, Weidemann BJ, Castro AN, Walsh JW, deLeon O, Burnett CML, Pearson NA, Murry DJ, Grobe JL, and Kirby JR (2015). Risperidone-induced weight gain is mediated through shifts in the gut microbiome and suppression of energy expenditure. EBioMedicine 2, 1725–1734. [PubMed: 26870798]

Ballsmider LA, Vaughn AC, David M, Hajnal A, Di Lorenzo PM, and Czaja K (2015). Sleeve gastrectomy and Roux-en-Y gastric bypass alter the gut-brain communication. Neural Plast. 2015, 601985. [PubMed: 25722893]

Baron R, Janig W, and McLachlan EM (1985). The afferent and sympathetic components of the lumbar spinal outflow to the colon and pelvic organs in the cat. III. The colonic nerves, incorporating an analysis of all components of the lumbar prevertebral outflow. J. Comp. Neurol. 238, 158–168. [PubMed: 4044909]

Berthoud HR, Blackshaw LA, Brookes SJ, and Grundy D (2004). Neuroanatomy of extrinsic afferents supplying the gastrointestinal tract. Neurogastroenterol. Motil. 16 (Suppl 1), 28–33. [PubMed: 15066001]

Buchwald H, and Oien DM (2013). Metabolic/bariatric surgery worldwide 2011. Obes. Surg. 23, 427–436. [PubMed: 23338049]

Buchwald H, Avidor Y, Braunwald E, Jensen MD, Pories W, Fahrbach K, and Schoelles K (2004). Bariatric surgery: a systematic review and metaanalysis. JAMA 292, 1724–1737. [PubMed: 15479938]

Burnett CM, and Grobe JL (2013). Direct calorimetry identifies deficiencies in respirometry for the determination of resting metabolic rate in C57Bl/6 and FVB mice. Am. J. Physiol. Endocrinol. Metab. 305, E916–E924. [PubMed: 23964071]

Burnett CM, and Grobe JL (2014). Dietary effects on resting metabolic rate in C57BL/6 mice are differentially detected by indirect (O2/CO2 respirometry) and direct calorimetry. Mol. Metab. 3, 460–464. [PubMed: 24944905]

Cammisotto P, and Bendayan M (2012). A review on gastric leptin: the exocrine secretion of a gastric hormone. Anat. Cell Biol. 45, 1–16. [PubMed: 22536547]

Cardinal P, André C, Quarta C, Bellocchio L, Clark S, Elie M, Leste-Lasserre T, Maitre M, Gonzales D, Cannich A, et al. (2014). CB1 cannabinoid receptor in SF1-expressing neurons of the ventromedial hypothalamus determines metabolic responses to diet and leptin. Mol. Metab. 3, 705–716. [PubMed: 25352999]

Chambers AP, Kirchner H, Wilson-Perez HE, Willency JA, Hale JE, Gaylinn BD, Thorner MO, Pfluger PT, Gutierrez JA, Tschöp MH, et al. (2013). The effects of vertical sleeve gastrectomy in rodents are ghrelin independent. Gastroenterology 144, 50–52.e5. [PubMed: 22995675]

Conceição E, Bastos AP, Brandão I, Vaz AR, Ramalho S, Arrojado F, da Costa JM, and Machado PP (2014). Loss of control eating and weight outcomes after bariatric surgery: a study with a Portuguese sample. Eat. Weight Disord. 19, 103–109. [PubMed: 24065351]

DiPatrizio NV, Astarita G, Schwartz G, Li X, and Piomelli D (2011). Endocannabinoid signal in the gut controls dietary fat intake. Proc. Natl. Acad. Sci. USA 108, 12904–12908. [PubMed: 21730161]

DiPatrizio NV, Joslin A, Jung KM, and Piomelli D (2013). Endocannabinoid signaling in the gut mediates preference for dietary unsaturated fats. FASEB J. 27, 2513–2520. [PubMed: 23463697]

Drucker DJ (2007). The role of gut hormones in glucose homeostasis. J. Clin. Invest. 117, 24–32. [PubMed: 17200703]

Farooqi IS, and O'Rahilly S (2009). Leptin: a pivotal regulator of human energy homeostasis. Am. J. Clin. Nutr. 89, 980S–984S. [PubMed: 19211814]

Gautron L, Zechner JF, and Aguirre V (2013). Vagal innervation patterns following Roux-en-Y gastric bypass in the mouse. Int. J. Obes. 37, 1603–1607.

Gómez R, Navarro M, Ferrer B, Trigo JM, Bilbao A, Del Arco I, Cippitelli A, Nava F, Piomelli D, and Rodríguez de Fonseca F (2002). A peripheral mechanism for CB1 cannabinoid receptor-dependent modulation of feeding. J. Neurosci. 22, 9612–9617. [PubMed: 12417686]

González-Muniesa P, Mártinez-González MA, Hu FB, Després JP, Matsuzawa Y, Loos RJF, Moreno LA, Bray GA, and Martinez JA (2017). Obesity. Nat. Rev. Dis. Primers 3, 17034. [PubMed: 28617414]

Han B, Compton WM, Blanco C, and Jones CM (2019). Time since first cannabis use and 12-month prevalence of cannabis use disorder among youth and emerging adults in the United States. Addiction 114, 698–707. [PubMed: 30474910]

Hao Z, Townsend RL, Mumphrey MB, Patterson LM, Ye J, and Berthoud HR (2014). Vagal innervation of intestine contributes to weight loss After Roux-en-Y gastric bypass surgery in rats. Obes. Surg. 24, 2145–2151. [PubMed: 24972684]

Hao Z, Townsend RL, Mumphrey MB, Morrison CD, Münzberg H, and Berthoud HR (2017). RYGB Produces more Sustained Body Weight Loss and Improvement of Glycemic Control Compared with VSG in the Diet-Induced Obese Mouse Model. Obes. Surg. 27, 2424–2433. [PubMed: 28386755]

Heinberg LJ, Ashton K, and Windover A (2010). Moving beyond dichotomous psychological evaluation: the Cleveland Clinic Behavioral Rating System for weight loss surgery. Surg. Obes. Relat. Dis. 6, 185–190. [PubMed: 20096644]

Jeraldo P, Kalari K, Chen X, Bhavsar J, Mangalam A, White B, Nelson H, Kocher JP, and Chia N (2014). IM-TORNADO: a tool for comparison of 16S reads from paired-end libraries. PLoS ONE 9, e114804. [PubMed: 25506826]

Liou AP, Paziuk M, Luevano JM Jr., Machineni S, Turnbaugh PJ, and Kaplan LM (2013). Conserved shifts in the gut microbiota due to gastric bypass reduce host weight and adiposity. Sci. Transl. Med. 5, 178ra41.

Lipina C, Macrae K, Suhm T, Weigert C, Blachnio-Zabielska A, Baranowski M, Gorski J, Burgess K, and Hundal HS (2013). Mitochondrial substrate availability and its role in lipid-induced insulin resistance and proinflammatory signaling in skeletal muscle. Diabetes 62, 3426–3436. [PubMed: 23733201]

López M, Diéguez C, and Nogueiras R (2015). Hypothalamic GLP-1: the control of BAT thermogenesis and browning of white fat. Adipocyte 4, 141–145. [PubMed: 26167417]

Maciejewski ML, Arterburn DE, Van Scoyoc L, Smith VA, Yancy WS Jr., Weidenbacher HJ, Livingston EH, and Olsen MK (2016). Bariatric Surgery and Long-term Durability of Weight Loss. JAMA Surg. 151, 1046–1055. [PubMed: 27579793]

Mehrpouya-Bahrami P, Chitrala KN, Ganewatta MS, Tang C, Murphy EA, Enos RT, Velazquez KT, McCellan J, Nagarkatti M, and Nagarkatti P (2017). Blockade of CB1 cannabinoid receptor alters gut microbiota and attenuates inflammation and diet-induced obesity. Sci. Rep. 7, 15645. [PubMed: 29142285]

Mokadem M, Zechner JF, Margolskee RF, Drucker DJ, and Aguirre V (2013). Effects of Roux-en-Y gastric bypass on energy and glucose homeostasis are preserved in two mouse models of functional glucagon-like peptide-1 deficiency. Mol. Metab. 3, 191–201. [PubMed: 24634822]

Mokadem M, Zechner JF, Uchida A, and Aguirre V (2015). Leptin Is Required for Glucose Homeostasis after Roux-en-Y Gastric Bypass in Mice. PLoS ONE 10, e0139960. [PubMed: 26445459]

Moreno-Navarrete JM, Serino M, Blasco-Baque V, Azalbert V, Barton RH, Cardellini M, Latorre J, Ortega F, Sabater-Masdeu M, Burcelin R, et al. (2018). Gut Microbiota Interacts with Markers of Adipose Tissue Browning, Insulin Action and Plasma Acetate in Morbid Obesity. Mol. Nutr. Food Res. 62, 1–9.

Murphy KG, and Bloom SR (2006). Gut hormones and the regulation of energy homeostasis. Nature 444, 854–859. [PubMed: 17167473]

Nakano M, Goris RC, Atobe Y, Kadota T, and Funakoshi K (2009). Mediolateral and rostrocaudal topographic organization of the sympathetic pre-ganglionic cell pool in the spinal cord of Xenopus laevis. J. Comp. Neurol. 513, 292–314. [PubMed: 19148922]

Neinast MD, Frank AP, Zechner JF, Li Q, Vishvanath L, Palmer BF, Aguirre V, Gupta RK, and Clegg DJ (2015). Activation of natriuretic peptides and the sympathetic nervous system following Roux-en-Y gastric bypass is associated with gonadal adipose tissues browning. Mol. Metab. 4, 427–436. [PubMed: 25973390]

Odom J, Zalesin KC, Washington TL, Miller WW, Hakmeh B, Zaremba DL, Altattan M, Balasubramaniam M, Gibbs DS, Krause KR, et al. (2010). Behavioral predictors of weight regain after bariatric surgery. Obes. Surg. 20, 349–356. [PubMed: 19554382]

Okafor PN, Lien C, Bairdain S, Simonson DC, Halperin F, Vernon AH, Linden BC, and Lautz DB (2015). Effect of vagotomy during Roux-en-Y gastric bypass surgery on weight loss outcomes. Obes. Res. Clin. Pract. 9, 274–280. [PubMed: 25458372]

Penney NC, Kinross J, Newton RC, and Purkayastha S (2015). The role of bile acids in reducing the metabolic complications of obesity after bariatric surgery: a systematic review. Int. J. Obes. 39, 1565–1574.

Pittet P, Gygax PH, and Jéquier E (1974). Thermic effect of glucose and amino acids in man studied by direct and indirect calorimetry. Br. J. Nutr. 31, 343–349. [PubMed: 4835787]

Pittet P, Chappuis P, Acheson K, De Techtermann F, and Jéquier E (1976). Thermic effect of glucose in obese subjects studied by direct and indirect calorimetry. Br. J. Nutr. 35, 281–292. [PubMed: 1252403]

Puzziferri N, Roshek TB 3rd, Mayo HG, Gallagher R, Belle SH, and Livingston EH (2014). Long-term follow-up after bariatric surgery: a systematic review. JAMA 312, 934–942. [PubMed: 25182102]

Quarta C, Bellocchio L, Mancini G, Mazza R, Cervino C, Braulke LJ, Fekete C, Latorre R, Nanni C, Bucci M, et al. (2010). CB(1) signaling in forebrain and sympathetic neurons is a key determinant of endocannabinoid actions on energy balance. Cell Metab. 11, 273–285. [PubMed: 20374960]

Riedl RA, Atkinson SN, Burnett CML, Grobe JL, and Kirby JR (2017). The Gut Microbiome, Energy Homeostasis, and Implications for Hypertension. Curr. Hypertens. Rep. 19, 27. [PubMed: 28316052]

Ryan KK, Tremaroli V, Clemmensen C, Kovatcheva-Datchary P, Myronovych A, Karns R, Wilson-Pérez HE, Sandoval DA, Kohli R, Bäckhed F, and Seeley RJ (2014). FXR is a molecular target for the effects of vertical sleeve gastrectomy. Nature 509, 183–188. [PubMed: 24670636]

Sam AH, Salem V, and Ghatei MA (2011). Rimonabant: From RIO to Ban. J. Obes. 2011, 432607. [PubMed: 21773005]

Sarwer DB, Cohn NI, Gibbons LM, Magee L, Crerand CE, Raper SE, Rosato EF, Williams NN, and Wadden TA (2004). Psychiatric diagnoses and psychiatric treatment among bariatric surgery candidates. Obes. Surg. 14, 1148–1156. [PubMed: 15527626]

Schauer PR, Bhatt DL, Kirwan JP, Wolski K, Aminian A, Brethauer SA, Navaneethan SD, Singh RP, Pothier CE, Nissen SE, and Kashyap SR; STAMPEDE Investigators (2017). Bariatric Surgery versus Intensive Medical Therapy for Diabetes - 5-Year Outcomes. N. Engl. J. Med. 376, 641–651. [PubMed: 28199805]

Seeley RJ, Chambers AP, and Sandoval DA (2015). The role of gut adaptation in the potent effects of multiple bariatric surgeries on obesity and diabetes. Cell Metab. 21, 369–378. [PubMed: 25662404]

Sjöström L, Narbro K, Sjöström CD, Karason K, Larsson B, Wedel H, Lystig T, Sullivan M, Bouchard C, Carlsson B, et al.; Swedish Obese Subjects Study (2007). Effects of bariatric surgery on mortality in Swedish obese subjects. N. Engl. J. Med. 357, 741–752. [PubMed: 17715408]

Staels B, and Fonseca VA (2009). Bile acids and metabolic regulation: mechanisms and clinical responses to bile acid sequestration. Diabetes Care 32 (Suppl 2), S237–S245. [PubMed: 19875558]

Stefater MA, Perez-Tilve D, Chambers AP, Wilson-Perez HE, Sandoval DA, Berger J, Toure M, Tschop M, Woods SC, and Seeley RJ (2010). Sleeve gastrectomy induces loss of weight and fat mass in obese rats, but does not affect leptin sensitivity. Gastroenterology 138, 2426–2436. [PubMed: 20226189]

Stefater MA, Wilson-Pérez HE, Chambers AP, Sandoval DA, and Seeley RJ (2012). All bariatric surgeries are not created equal: insights from mechanistic comparisons. Endocr. Rev. 33, 595–622. [PubMed: 22550271]

Sturm R, and Hattori A (2013). Morbid obesity rates continue to rise rapidly in the United States. Int. J. Obes. 37, 889–891.

Tam CS, Redman LM, Greenway F, LeBlanc KA, Haussmann MG, and Ravussin E (2016). Energy Metabolic Adaptation and Cardiometabolic Improvements One Year After Gastric Bypass, Sleeve Gastrectomy, and Gastric Band. J. Clin. Endocrinol. Metab. 101, 3755–3764. [PubMed: 27490919]

Thivel D, Brakonieki K, Duche P, Morio B, Boirie Y, and Laferrère B (2013). Surgical weight loss: impact on energy expenditure. Obes. Surg. 23, 255–266. [PubMed: 23224568]

Tremaroli V, Karlsson F, Werling M, Ståhlman M, Kovatcheva-Datchary P, Olbers T, Fändriks L, le Roux CW, Nielsen J, and Bäckhed F (2015). Roux-en-Y Gastric Bypass and Vertical Banded

Gastroplasty Induce Long-Term Changes on the Human Gut Microbiome Contributing to Fat Mass Regulation. Cell Metab. 22, 228–238. [PubMed: 26244932]

Tschöp MH, Speakman JR, Arch JRS, Auwerx J, Brüning JC, Chan L, Eckel RH, Farese RV Jr., Galgani JE, Hambly C, et al. (2011). A guide to analysis of mouse energy metabolism. Nat. Methods 9, 57–63. [PubMed: 22205519]

van Beek AP, Emous M, Laville M, and Tack J (2017). Dumping syndrome after esophageal, gastric or bariatric surgery: pathophysiology, diagnosis, and management. Obes. Rev. 18, 68–85. [PubMed: 27749997]

Walsberg GE, and Hoffman TC (2005). Direct calorimetry reveals large errors in respirometric estimates of energy expenditure. J. Exp. Biol. 208, 1035–1043. [PubMed: 15767305]

Watanabe M, Houten SM, Mataki C, Christoffolete MA, Kim BW, Sato H, Messaddeq N, Harney JW, Ezaki O, Kodama T, et al. (2006). Bile acids induce energy expenditure by promoting intracellular thyroid hormone activation. Nature 439, 484–489. [PubMed: 16400329]

Watanabe M, Horai Y, Houten SM, Morimoto K, Sugizaki T, Arita E, Mataki C, Sato H, Tanigawara Y, Schoonjans K, et al. (2011). Lowering bile acid pool size with a synthetic farnesoid X receptor (FXR) agonist induces obesity and diabetes through reduced energy expenditure. J. Biol. Chem. 286, 26913–26920. [PubMed: 21632533]

Worthmann A, John C, Rühlemann MC, Baguhl M, Heinsen FA, Schaltenberg N, Heine M, Schlein C, Evangelakos I, Mineo C, et al. (2017).Cold-induced conversion of cholesterol to bile acids in mice shapes the gut microbiome and promotes adaptive thermogenesis. Nat. Med. 23, 839–849. [PubMed: 28604703]

Zechner JF, Mirshahi UL, Satapati S, Berglund ED, Rossi J, Scott MM, Still CD, Gerhard GS, Burgess SC, Mirshahi T, et al. (2013). Weight-independent effects of roux-en-Y gastric bypass on glucose homeostasis via melanocortin-4 receptors in mice and humans. Gastroenterology 144, 580–590. [PubMed: 23159449]

Zhang Y, Proenca R, Maffei M, Barone M, Leopold L, and Friedman JM (1994). Positional cloning of the mouse obese gene and its human homologue. Nature 372, 425–432. [PubMed: 7984236]

Zou S, and Kumar U (2018). Cannabinoid Receptors and the Endocannabinoid System: Signaling and Function in the Central Nervous System. Int. J. Mol. Sci. 19, 833.

Highlights

- RYGB, but not SG, increases energy expenditure (EE) and RMR
- This increase in EE is due to sympathetic-mediated “browning” of mesenteric fat
- CB1 inverse agonist induces splanchnic nerve activity and fat thermogenesis
- CB1 agonist attenuates the RYGB-induced weight loss and “browning” of mesenteric fat

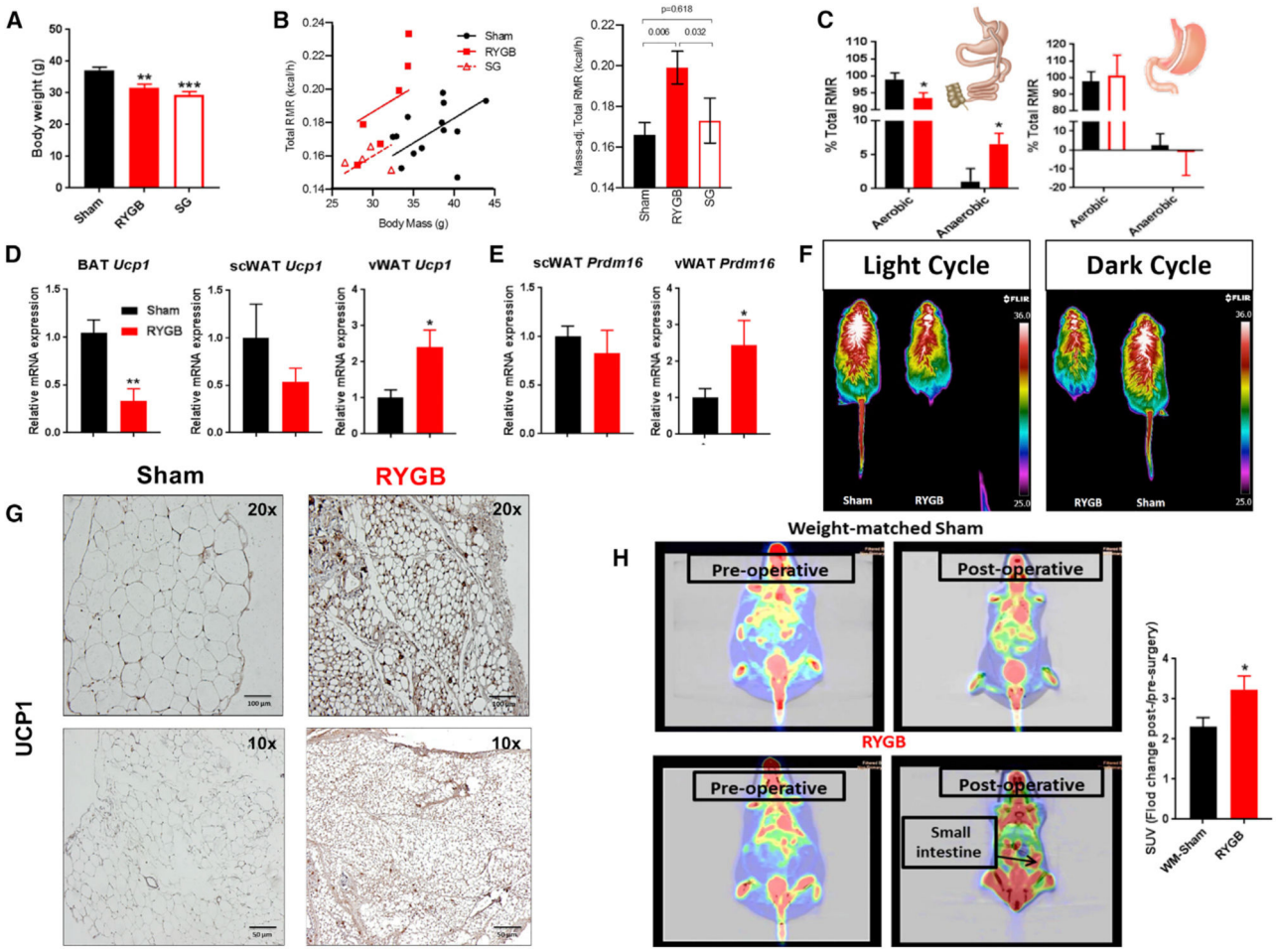

Figure 1. Increase in Energy Requirement and Thermogenic Activity of the Gut and Visceral Mesenteric Fat after RYGB

(A) Average body weights of RYGB- and SG-operated mice—2 weeks after surgery—before undergoing resting metabolic rate (RMR) measurements using a combined direct and indirect calorimeter. One-way ANOVA followed by Tukey's test, **p < 0.01, ***p < 0.001, RYGB/SG versus sham.

(B) Total RMR (kcal/h measured by direct calorimetry in RYGB-, SG-, and sham-operated mice) corrected for weight factor with analysis of covariance (ANCOVA).

(C) Anaerobic RMR—calculated from total RMR (measured by direct calorimetry) and aerobic RMR (measured by respirometry or indirect calorimetry)—in RYGB- and SG-operated mice. Aerobic and anaerobic RMR expressed as percentage of total RMR in RYGB and SG mice. *p < 0.05, **p < 0.01 RYGB versus sham; #p < 0.05 RYGB versus SG (B and C). Mean ± SEM. Sham n = 13, RYGB n = 6, SG n = 4–5 (A–C).

(D) Relative *Ucp1* mRNA expression in brown adipose tissue (BAT), visceral mesenteric white adipose tissue (vWAT), and subcutaneous white adipose tissue (scWAT) of RYGB- versus sham-operated mice.

(E) Relative *Prdm16* mRNA expression in vWAT and scWAT of RYGB- versus sham-operated mice.

(F) *In vivo* recording of surface body temperature by infrared camera in RYGB- and sham-operated mice while on light treadmill exercise during light and dark cycles (4 weeks after surgery).
(G) UCP1 protein expression—assessed by immunohistochemistry (IHC)—in the vWAT of DIO mice 5 weeks post-RYGB surgery. Scale bar, 100 μm (top); 50 μm (bottom).
(H) ^{18}Fluoro-deoxyglucose (FDG) uptake analysis under positron emission tomography (PET) scan imaging before and after surgery in RYGB-operated mice and weight-matched sham (WM-sham) counterparts. Average standardized uptake values (SUVs) of the small intestine in RYGB and WM-sham. Mean ± SEM. Sham n = 7–9, RYGB n = 6–8. *$p < 0.05$, **$p < 0.01$ RYGB versus sham or WM-sham by t test (D–H).

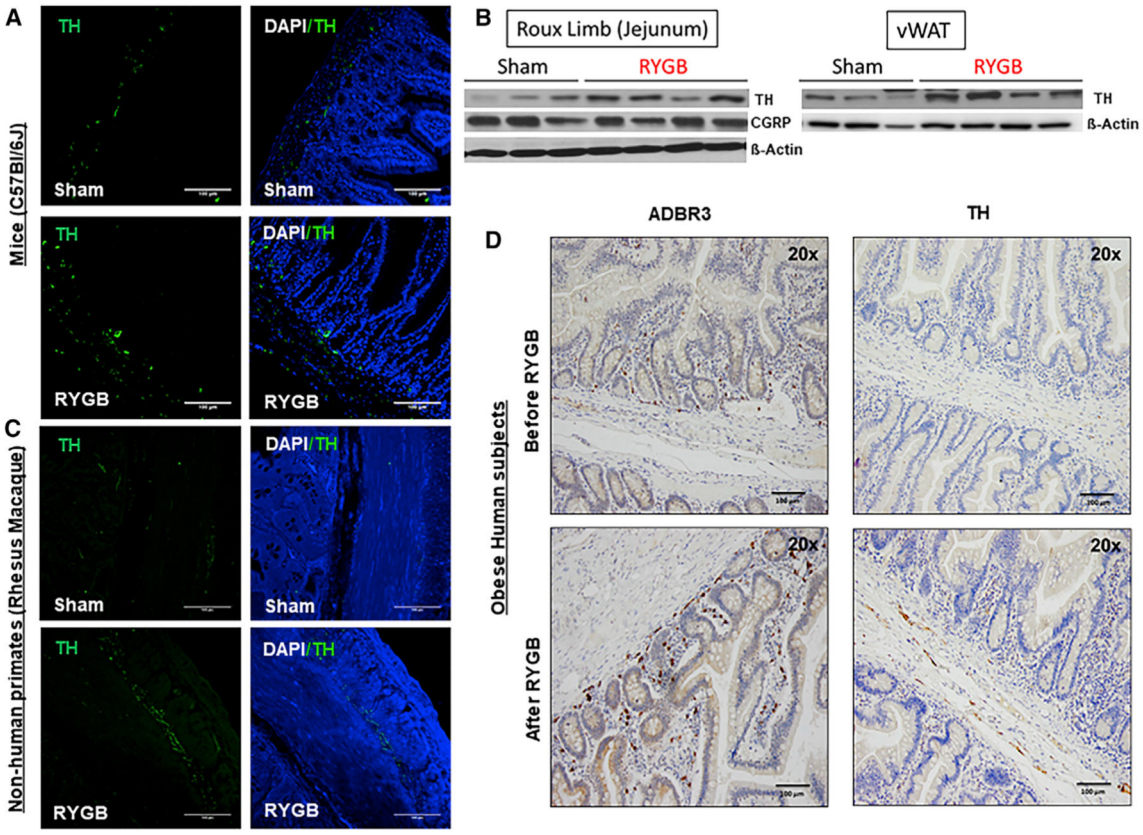

Figure 2. RYGB Induces an Increase in Markers of Gut's Sympathetic Nerve Activity

(A) TH expression—assessed by immunofluorescence (IF)—in the Roux limb (or jejunum) of DIO C57BL/6 mice after RYGB compared with their sham counterparts 6 weeks after surgery. Sham n = 5, RYGB n = 5.

(B) TH and CGRP expression—assessed by western blot—within the Roux limb (jejunum) as well as TH expression within vWAT of RYGB- and sham-operated DIO mice 6 weeks after surgery. β-Actin serviced as a loading control.

(C) TH expression—assessed by IF—in the Roux limb (or jejunum) of DIO rhesus macaque monkeys after RYGB compared with their sham counterparts 12 weeks after surgery. Sham n = 4, RYGB n = 4.

(D) ADBR3 and TH expression in Roux (or proximal jejunum)—assessed by IHC—of obese human subjects at time of surgery (before RYGB) and 1–5 years afterward (after RYGB). n = 4–5. Scale bar, 100 μm (A, C, and D).

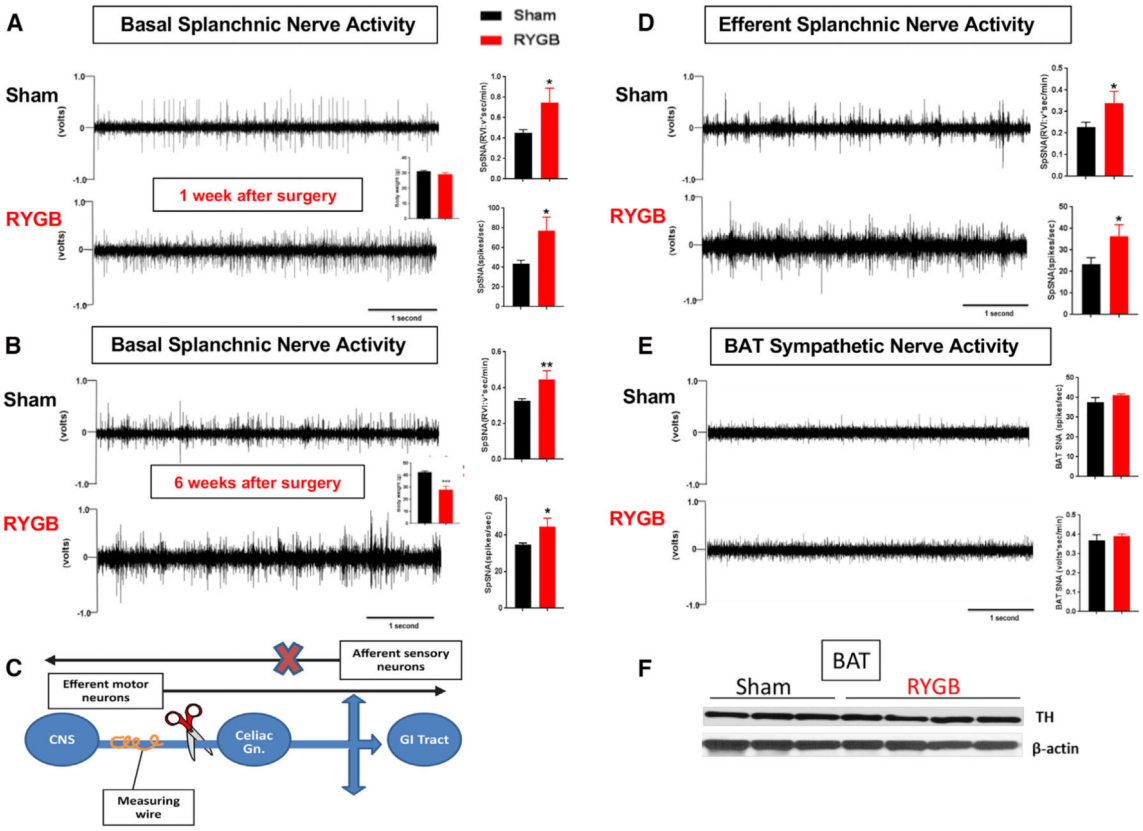

Figure 3. Increase in SNA of the Small Intestine after RYGB

(A and B) Direct multi-fiber recording of basal splanchnic sympathetic nerve activity (SpSNA), expressed as volts*s/min or spikes/s in DIO mice 1 week (A) and 6 weeks (B) after RYGB (quantification in the adjacent graph).

(C) Schematic illustration of acute “de-afferentation” (i.e., elimination of afferent neuron fibers) as performed to measure the activity of the sympathetic efferent fibers of the splanchnic nerve.

(D) Direct recording of the activity of the splanchnic efferent fibers in RYGB- and sham-operated mice measured 60 min after acute “de-afferentation” of the greater splanchnic nerve causing loss of the afferent sensory fibers (quantification in the adjacent graph).

(E) BAT SNA (expressed in RVI = volts*s/min and in frequency = spikes/s) in RYGB- and sham-operated mice (6 weeks after surgery) (quantification in the adjacent graph).

(F) TH expression assessed by western blot in BAT of RYGB- and sham-operated DIO mice (6 weeks after surgery). Mean ± SEM. Sham n = 5–6, RYGB n = 5–6. *p < 0.05, **p < 0.01 RYGB versus sham by t test.

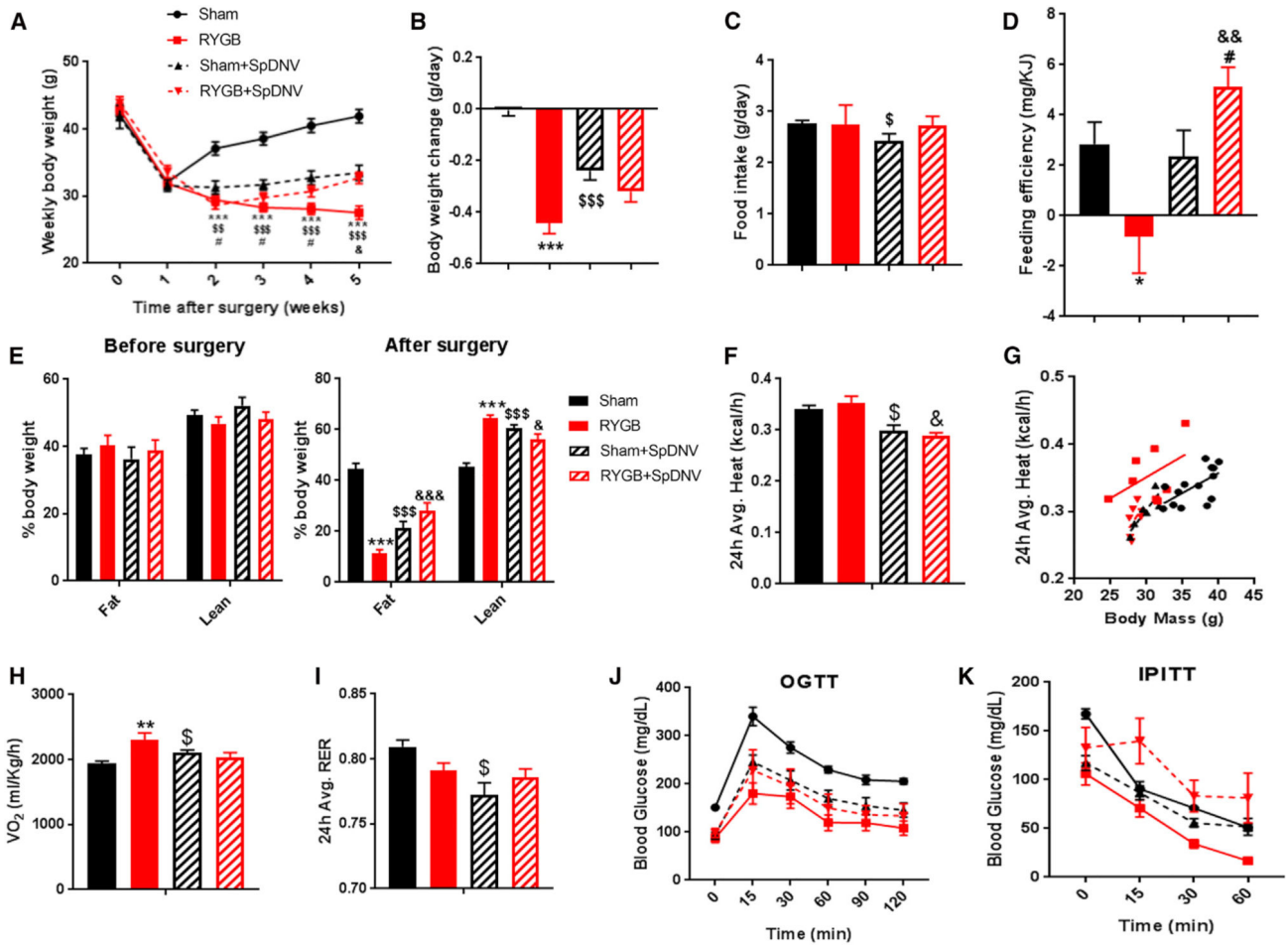

Figure 4. SpDNV Eliminates All Metabolic-Proven Effects of RYGB

(A) Average weekly body weight in g of RYGB-operated DIO mice with and without selective splanchnic denervation (SpDNV) compared with their sham counterparts.

(B) Change in body weight (g/day) over 5 weeks after RYGB.

(C) Average daily food intake.

(D) Feeding efficiency (expressed as mg of body weight gain per kJ consumed).

(E) Fat and lean mass—assessed by NMR—before and after surgeries.

(F–I) Total energy expenditure (F and G), O_2 consumption (H), and respiratory exchange ratio (RER) (I) were all obtained from measurements taken during the CLAMS system using respirometry or indirect calorimetry in free-moving animals.

(J and K) Oral glucose tolerance test (J) and insulin tolerance test (K) performed during post-operative week 4 or 5 in RYGB- and sham-operated mice with or without SpDNV. Mean ± SEM. Sham n = 11, RYGB n = 9, sham + SpDNV n = 8, RYGB + SpDNV n = 9. ANOVA followed by Tukey's test. $^{*, \#, \$}p < 0.05$; $^{\$\$, \&\&}p < 0.01$; $^{***, \$\$\$}p < 0.001$. *Sham versus RYGB; #sham + SpDNV versus RYGB + SpDNV; $^{\$}$sham versus sham + SpDNV; $^{\&}$RYGB versus RYGB + SpDNV.

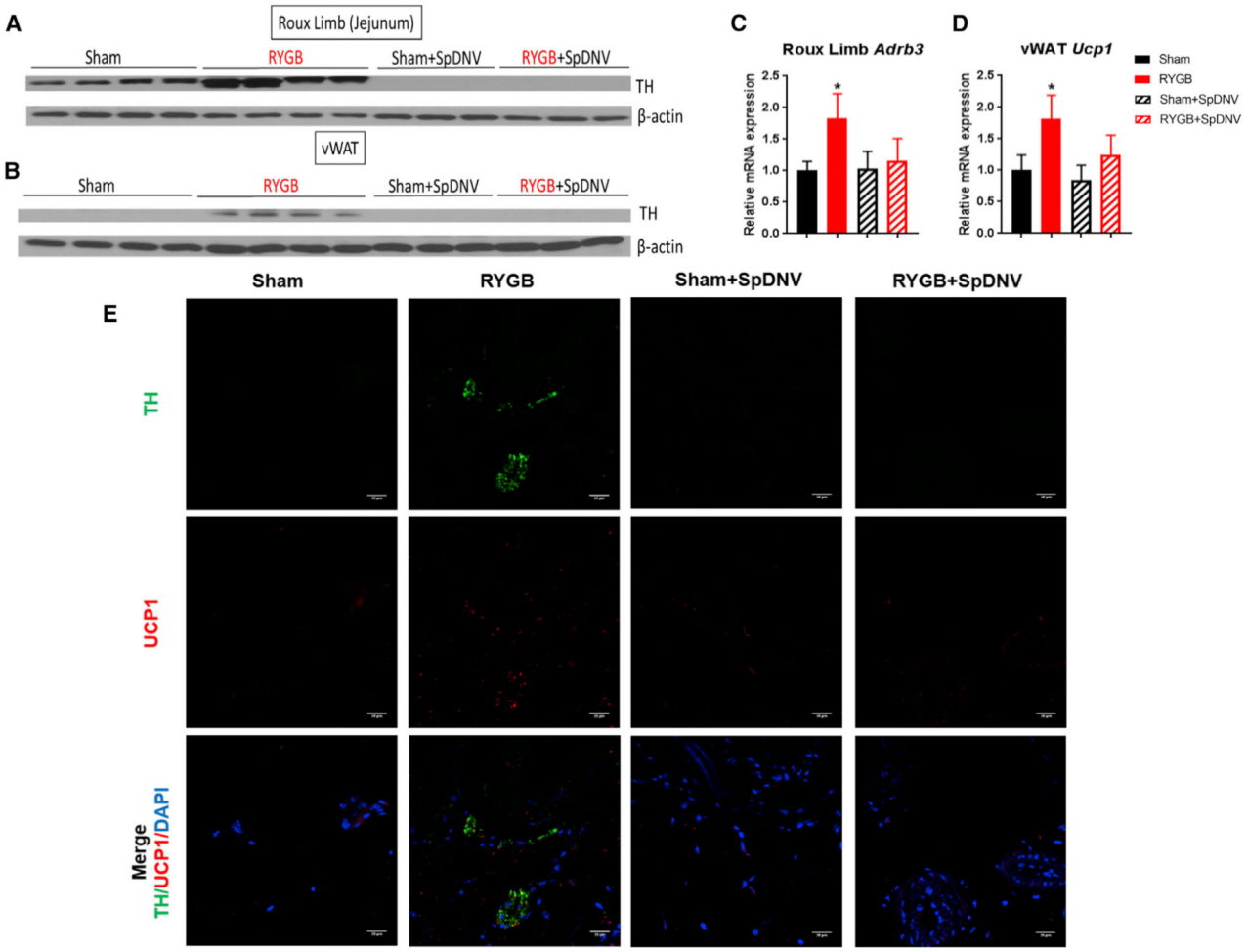

Figure 5. Selective SpDNV Abolishes the RYGB-Induced Increase in Markers of SNA, Thermogenesis, and Co-localization of TH and UCP1 within vWAT

(A and B) TH protein expression, assessed by western blot, in the Roux limb (jejunum) (A) and vWAT (B) among sham-, RYGB-, sham- + SpDNV-, and RYGB- + SpDNV-operated DIO male mice 6 weeks after surgery.

(C and D) Relative *Adrb3* mRNA expression within the Roux limb (jejunum) (C) and *Ucp1* mRNA expression within the vWAT (D) of RYGB- and sham-operated DIO mice with or without SpDNV. Mean ± SEM. Sham n = 11, RYGB n = 9, sham + SpDNV n = 8, RYGB + SpDNV n = 9. ANOVA followed by Tukey's test. *$p < 0.05$, sham versus RYGB.

(E) TH and UCP1 co-expression—assessed by IF—within vWAT of DIO mice after RYGB compared with their sham counterparts with or without SpDNV 6 weeks after surgery. DAPI = blue, TH = green, UCP1 = red. Scale bar, 100 μm.

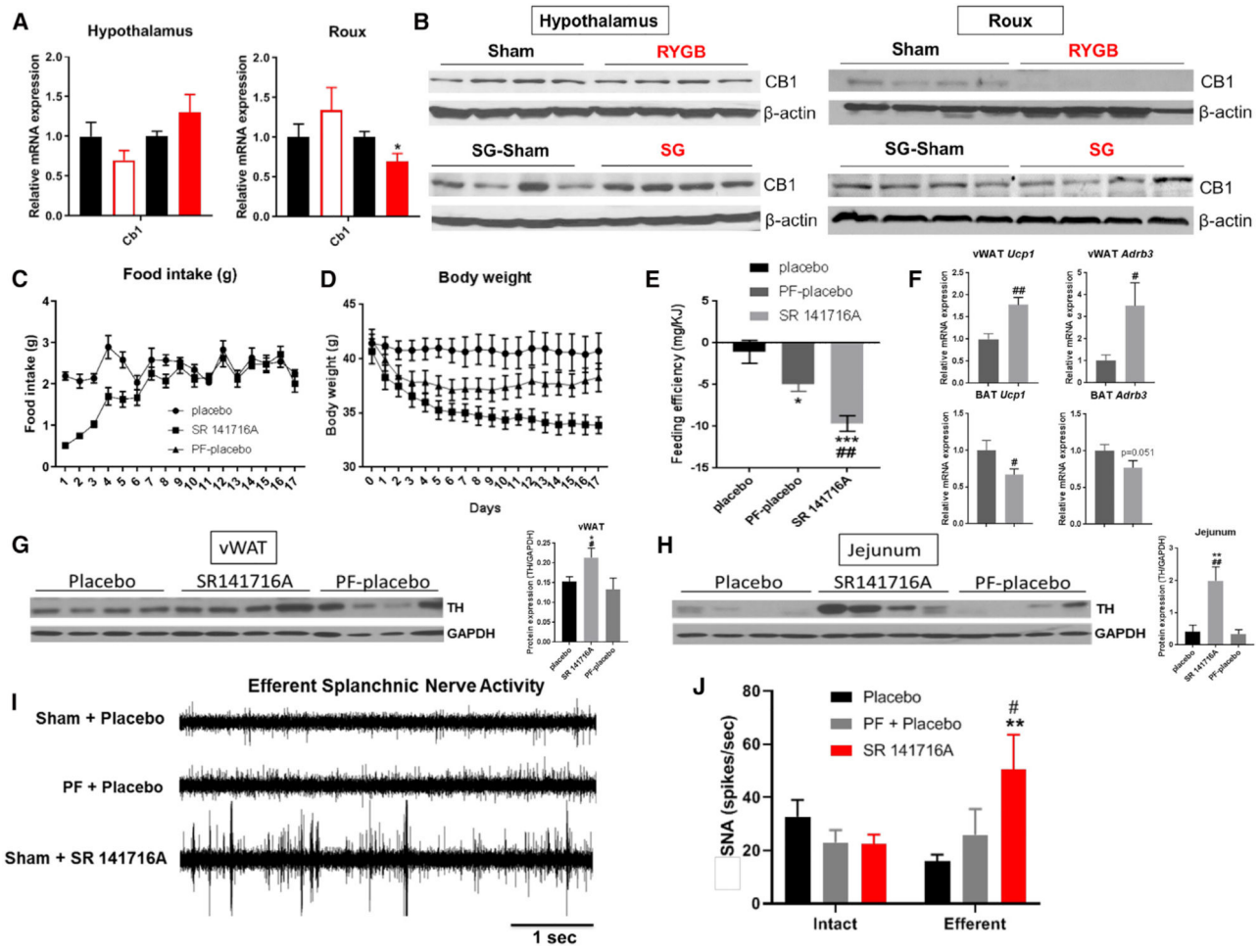

Figure 6. RYGB, but Not SG, Decreases Intestinal CB1 Expression, and CB1 Inverse Agonist (SR141716A) Mimics the Effect of RYGB on Energy Balance and Splanchnic Nerve Activity

(A and B) Relative *Cb1* mRNA expression (A) and CB1 protein expression (B)—assessed by western blot—in the hypothalamus and Roux limb (jejunum) of RYGB- and SG-operated mice compared with their sham counterparts. RYGB n = 8, RYGB-sham n = 8, SG n = 6, SG-sham n = 6. *$p < 0.05$, sham versus RYGB or SG-sham versus SG by t test.

(C–E) Average daily food intake (C), body weight in g (D), and overall feeding efficiency (E) in single-housed DIO mice after daily oral gavage of 10 mg/kg SR141716A (closed square) or placebo (closed circle). A placebo group that was PF to the SR141716A group (PF-placebo) is shown in parallel to control for the effects of reduction in food intake (closed triangle). ANOVA followed by Tukey's test.

(F) Relative *Adrb3* and *Ucp1* mRNA expression in vWAT and BAT. t test.

(G and H) TH protein expression in vWAT (G) and jejunum (H) assessed by western blot. ANOVA followed by Tukey's test.

(I and J) A representative neurogram of efferent splanchnic nerve activity (I) and direct multi-fiber recording (J) of intact and efferent SNA, expressed as spikes/s in DIO mice after daily oral gavage of 10 mg/kg SR141716A versus placebo, or PF mice to the SR141716A group. Mean ± SEM. Sham + placebo n = 6, PF + placebo n = 6, sham + SR14716A n = 5–6. ANOVA followed by Tukey's test. *, #$p < 0.05$; **, ##$p < 0.01$; ***$p < 0.001$. *Compares

placebo versus PF-placebo or SR141716A; #compares PF-placebo versus SR141716A (C–J).

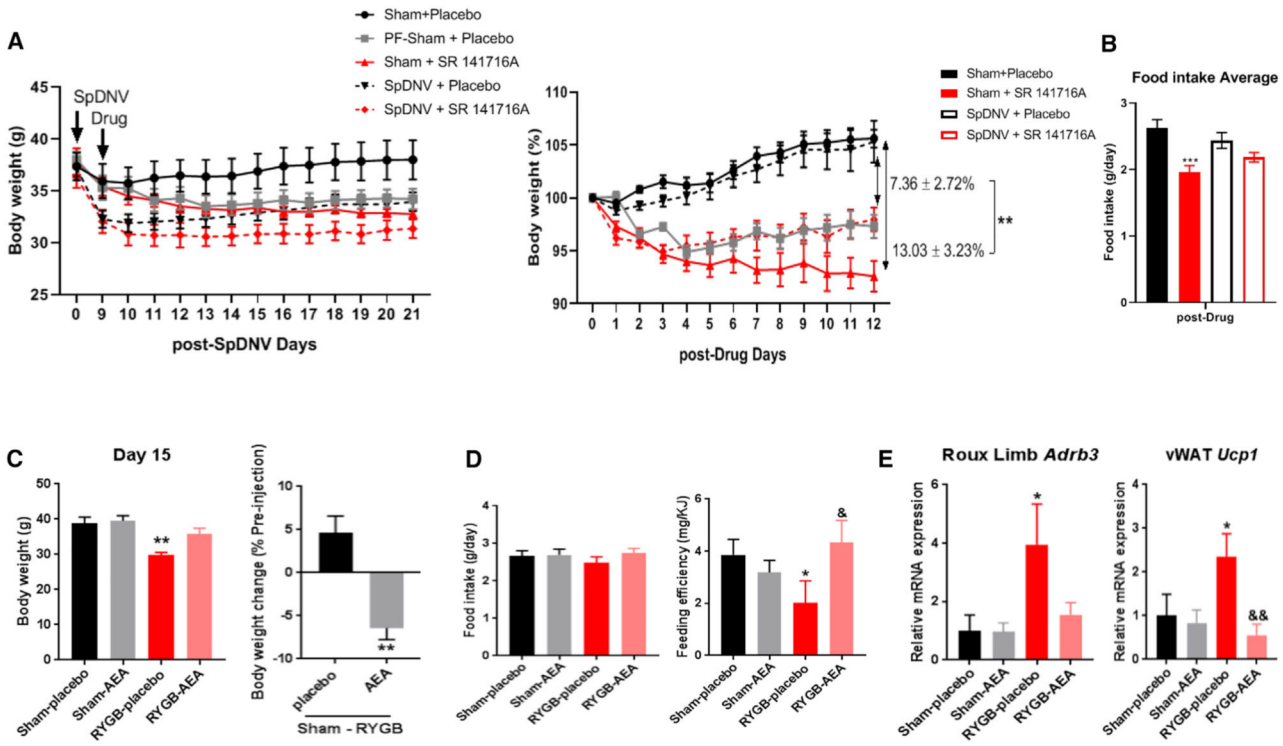

Figure 7. The Effect of CB1 Inverse Agonist (SR141716A) Is Attenuated after Splanchnic Denervation, while the CB1 Agonist (AEA) Mitigates the RYGB-Induced Changes in Energy Balance

(A and B) Daily administration of SR141716A versus placebo by oral gavage to male DIO mice with or without SpDNV. (A) Body weight expressed in g (graph to the left) and percentage of initial body weight at time of drug administration (graph to the right) over time (in days). (B) Average daily food intake (g/day) of male DIO mice treated with either SpDNV or sham surgery in combination with daily administration of 10 mg/kg SR141716A versus placebo. Mean ± SEM. n = 5–6. ANOVA followed by Tukey's test. **$p < 0.01$, ***$p < 0.001$.

(C–F) CB1 agonist (20 mg/kg) arachidonoylethanolamide (AEA) or sunflower oil (placebo) was administered daily by oral gavage—starting post-operative week 3—into RYGB- and sham-operated DIO mice for 15 consecutive days. (C) Body weight expressed in g (at day 15) in RYGB- and sham-operated mice receiving either placebo or AEA and percentage (%) change in body weight between RYGB- and sham-operated DIO mice after 15 days of placebo versus AEA treatment by t test. (D) Average daily food intake in g/day and feeding efficiency in (mg of body weight gain per kJ consumed) during gavage. (E) Relative *Adrb3* mRNA expression in Roux limb (jejunum) and *Ucp1* mRNA expression in vWAT in RYGB- and sham-operated mice treated with placebo or AEA. Mean ± SEM. n = 5–6. ANOVA followed by Tukey's test (D and E). *, &$p < 0.05$; **, &&$p < 0.01$. *Compares sham-placebo versus RYGB-placebo; &compares RYGB-placebo versus RYGB-AEA.

KEY RESOURCES TABLE

REAGENT or RESOURCE	SOURCE	IDENTIFIER
Antibodies		
Goat polyclonal anti-UCP1	Santa Cruz	Cat# sc-6528, RRID: AB_2304265
Rabbit polyclonal anti-Tyrosine Hydroxylase	PhosphoSolution	Cat# 2025-THRAB, RRID: AB_2492276
Rabbit polyclonal anti-CGRP	Sigma	Cat# C8198, RRID: AB_259091
Mouse monoclonal anti-β-actin	Proteintech	Cat# 60008–1-Ig, RRID: AB_2289225
Mouse monoclonal anti-GAPDH	Santa Cruz Biotechnology	Cat# sc-32233, RRID: AB_627679
Rabbit polyclonal anti-CB1	Abcam	Cat# ab23703, RRID: AB_447623
Alexa 488 goat anti-rabbit	Thermo Fisher Scientific	Cat# A32731, RRID: AB_2633280
Alexa 568 donkey anti-goat	Thermo Fisher Scientific	Cat# A-11057, RRID: AB_2534104
Biological Samples		
Human Jejunum samples (details in Table S1)	Paris Diderot University hospital, Paris, France	N/A
Human gastric samples (details in Table S2)	University of Iowa Hospitals and Clinics, Iowa City, IA	N/A
Chemicals, Peptides, and Recombinant Proteins		
Rimonabant (SR 141716A)	Tocris Bioscience	Cat# 0923, CAS: 158681–13-1
Rimonabant (SR 141716A)	Sigma	Cat# 0800–25mg
Arachidonylethanolamide Oil (AEA)	Sigma	Cat# A0580–25mg, CAS:94421–68-8
D-Glucose	RPI	CAS: 50–99-7
insulin (Humulin R)	Eli Lily	HI-210, NDC 0002–8215-01
silicone gel	World Precision Instruments	KWIK-SIL
Critical Commercial Assays		
Direct-zol RNA MiniPrep Plus kit	Zymo Research	Cat# R2072
cDNA High Capacity Reverse Transcription Kit	Applied Biosystems	Cat# 4368814
iQ™ SYBR® Green Supermix	Bio-Rad	Cat# 170–8882
Chemiluminescence (ECL) detection kit	GE Healthcare	Cat# RPN2232
Mouse metabolic kit	MSD	Cat# K15124C-1
U-PLEX Mouse PYY (total) Assay	MSD	Cat# K1526BK
Total bile acids kit	Crystal Chem	80470
Experimental Models: Organisms/Strains		
Mouse: Male DIO C57BL/6J	Jackson Laboratory	JAX: 380050
Mouse: Male C57BL/6J	Jackson Laboratory	JAX: 000664
Primates: Male Rhesus Macaques	Oregon National Primate Research Center, Beaverton, OR	N/A
Oligonucleotides		
β3-ADR Forward: GCC TTC CGTCGT GGT CTT CTG TG	Invitrogen	N/A
β3-ADR Reverse: GCC ATC AAA CCT GTT GAG C	Invitrogen	N/A
UCP1 Forward: GGA TGG TGA ACC CGA CAA C	Invitrogen	N/A

REAGENT or RESOURCE	SOURCE	IDENTIFIER
UCP1 Reverse: CTT GGA TCT GAA GGC GGA C	Invitrogen	N/A
PRDM16 Forward: GTA GCT GCT TCT GGG CTC A	IDT	N/A
PRDM16 Reverse: CGT CAC CGT CAC TTT TGG CT	IDT	N/A
CB1 Forward: GGG CAA ATT TCC TTG TAG CAG	IDT	N/A
CB1 Reverse: CTC AGT CTT TGA TTA GGC CAG G	IDT	N/A
rps18 Forward: CTG CCA TTA AGG GCG TGG	Invitrogen	N/A
rps18 reverse: TGA TCA CTC GCT CCA CCT CA	Invitrogen	N/A
Software and Algorithms		
ImageJ	NIH	https://imagej.nih.gov/ij/download.html
Graphpad prism 7.0	GraphPad Software	https://www.graphpad.com
Research IR software	FLIR	version 3.4.13039.1003
SPSS	IBM	https://www.ibm.com/products/spss-statistics
Other		
Thermal Imager	FLIR Systems	A655sc
bipolar platinum-iridium wire	A-M Systems	36-gauge
High impedance probe	Grass Instruments	HIP511
AC preamplifier	Grass Instruments	P5
Voltage integrator	University of Iowa Bioengineering	RVI: Model B600c
CLAMs system	Metabolic Phenotyping Core-University of Iowa	N/A
Combination of Direct and Indirect Calorimetry System	N/A	Burnett and Grobe, 2013; Walsberg and Hoffman, 2005
Bomb calorimetry	University of Arkansas Center of Excellence for Poultry Science, Fayetteville, AR	N/A
Nerve data acquisition system	MacLab	Model 8 s
Glucometer	Bayer HealthCare LLC	Contour
Catecholamine concentration (epinephrine (EPI) and norepinephrine (NE)) measurement	Vanderbilt University.	Hormone Assay and Analytical Resource Core